Title

THE SPECTRUM OF FOUR-TIMES IONIZED NIOBIUM, INCLUDING ZEEMAN STUDIES OF SELECTED LINES AND LASER MODIFICATION OF THE POPULATION OF CERTAIN LEVELS IN A SLIDING SPARK SOURCE

Author

Kagan, D.T.

Publication Date

1981-06-01

LBL-12822

Lawrence Berkeley Laboratory
UNIVERSITY OF CALIFORNIA

Materials & Molecular Research Division

THE SPECTRUM OF FOUR-TIMES IONIZED NIOBIUM, INCLUDING ZEEMAN STUDIES OF SELECTED LINES AND LASER MODIFICATION OF THE POPULATION OF CERTAIN LEVELS IN A SLIDING SPARK SOURCE

David Terry Kagan
(Ph.D. thesis)

June 1981

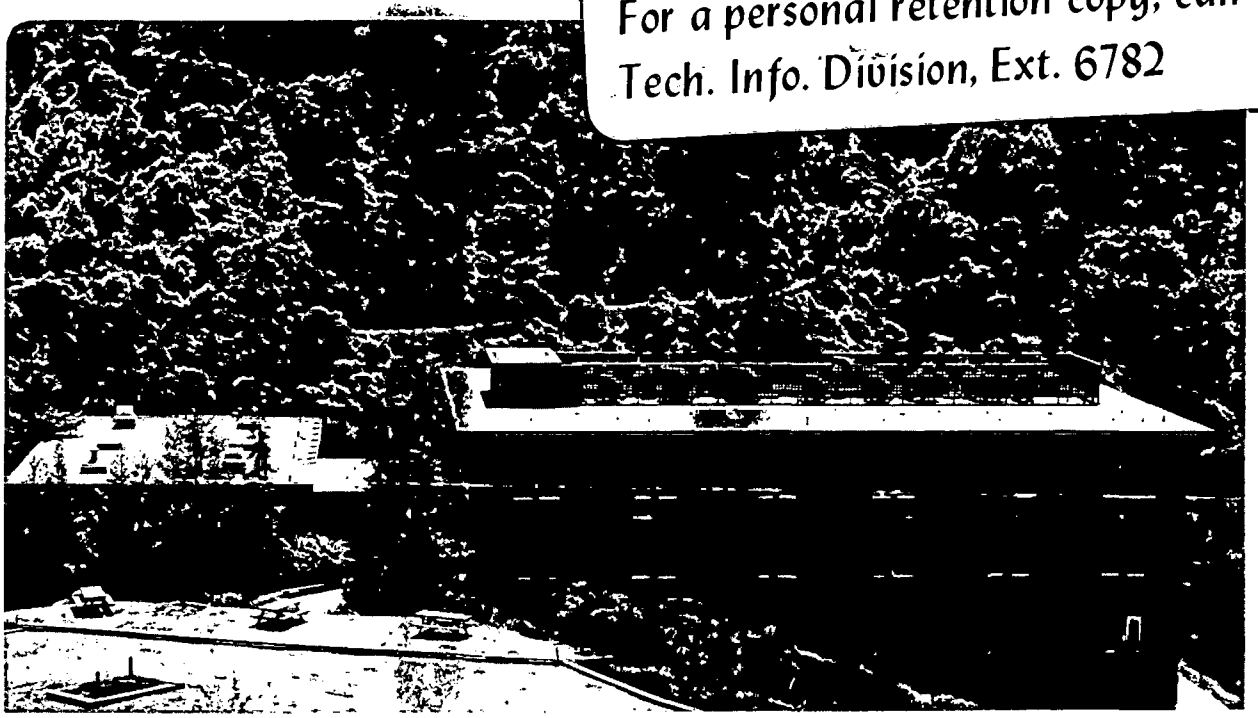

Prepared for the U.S. Department of Energy under Contract W-7405-ENG-48

LBL-12822

DISCLAIMER

LBL-12822

THE SPECTRUM OF FOUR-TIMES IONIZED NIOBIUM, INCLUDING ZEEMAN STUDIES OF SELECTED LINES AND LASER MODIFICATION OF THE POPULATION OF CERTAIN LEVELS IN A SLIDING SPARK SOURCE

David Terry Kagan

Department of Chemical Sciences
Materials and Molecular Research Division
Lawrence Berkeley Laboratory
University of California
Berkeley, California 94720

June 1981

This work was supported by the Director, Office of Energy Research, Office of Basic Energy Sciences, Chemical Sciences Division of the U.S. Department of Energy under Contract No. W-7405-ENG-48.

TABLE OF CONTENTS

LIST OF FIGURES

LIST OF TABLES

THE SPECTRUM OF FOUR-TIMES IONIZED NIOBIUM, INCLUDING ZEEMAN STUDIES OF SELECTED LINES AND LASER MODIFICATION OF THE POPULATION OF CERTAIN LEVELS IN A SLIDING SPARK SOURCE

David Terry Kagan

Department of Chemical Sciences
Materials and Molecular Research Division
Lawrence Berkeley Laboratory
University of California
Berkeley, California 94720

ABSTRACT

The $4p^6n\ell$ spectrum of Nb^{4+} was measured and analyzed. The spectrum was excited in a vacuum sliding spark source with a peak current of 800 amperes and a pulse width of 70 microseconds. The analysis of the spectrum has extended the 13 known lines to 84 and the 10 known levels to 30. The ionization energy was estimated to be 407897 cm^{-1}. There is strong evidence that the $4p^54d^2$ configuration interacts strongly with the $4p^6nf$ configuration. In addition, the hyperfine splitting of the $4p^66s$ level has been observed and measured to be 1.1 cm^{-1}.

An attempt was made to examine the Zeeman spectrum of selected lines of Nb^{4+}. However, the Doppler broadening of the lines prevented the acquisition of good results. A complete discussion of the Zeeman effect in the Nb^{4+} spectrum is contained in the text. In addition, the ability of a laser to modify the population of certain atomic levels in the sliding spark source was investigated. The completion of this experiment requires some new equipment.

I. INTRODUCTION

I.1. Spectroscopy - A Brief History

The science of spectroscopy originated with primitive man when he first began to wonder about the rainbow. However, this 'science' was more clearly characterized as mysticism. It was not until 1611 that the first nearly correct explanation of the rainbow was put forward by Archbishop Antonio de Dominis of Spalato.

Spectroscopy then had to wait nearly sixty years, for the genius of Sir Isaac Newton, to advance further. Newton's experiments with a glass prism and his explanation of those experiments would be the basis for the next 270 years of spectroscopy. In 1752, Thomas Melvill observed a sodium flame with a prism. This was the first study of an emission spectrum.

The next great contributions to spectroscopy were from Joseph Fraunhofer in 1814. Fraunhofer did a complete and detailed analysis of the spectrum of the sun. In addition, Fraunhofer was responsible for the invention of the diffraction grating. In 1859, Kirchoff formulated the law of emission and absorption which states: 'The relation between the powers of emission and absorption for rays of the same wavelength is constant for all bodies at the same temperature.' Kirchoff also recognized the connection between the spectrum of an object and its chemical composition, thus inventing the science of spectroscopic chemical analysis. The diffraction grating was improved immeasurably when Professor Henry Rowland of Johns Hopkins University perfected the ruling engine which allowed the production of diffraction gratings far superior to any

used previously. In addition, Rowland invented the concave grating which simplified and improved spectroscopic instruments.

Before the late nineteenth century, most of the advances in spectroscopy were technical. However, with the introduction of Balmer's law of the hydrogen spectra in 1885, the theoretical aspects of spectroscopy began an impressive series of advancements. In 1913, Bohr proposed his theory of the hydrogen atom. While he knew it had several faults, it was a master work because it gave the right answers for the spectra starting from something that at least resembled first principles. The understanding of atomic spectra became nearly complete as the theory of quantum mechanics developed in the early nineteen hundreds, however many interesting and important technical developments are still being attempted today.

For a more complete historical account of the history of spectroscopy see Sawyer [1946] or White [1934].

I.2. A Discussion on Four-Times Ionizied Niobium

Four-times ionized niobium (once called columbium) is the fifth member of the rubidium iso-electronic sequence. Its ground state electron configuration is a krypton noble gas core with a single additional electron. The lowest state for this additional electron turns out to be the 4d state instead of the 5s state, as in the first two members of the rubidium iso-electronic sequence.

Previous to this work, the fifth spectrum of niobium was investigated by M. W. Trawick [1934] and by G. W. Charles [1950]. From these two studies, the known spectrum of Nb V contained 13 lines and 10 levels.

The spectrum of four-times ionized niobium has two especially interesting features. The first is a dramatic perturbation in the $4p^6nf$ series which is most likely caused by configuration mixing with the $4p^54d5s$, $4p^54d^2$ or $4p^55s^2$ configuration. The strongest pertubation is due to the $4p^54d^2$ because it is the lowest energy configuration of these three. The second feature is a large hyperfine splitting in the S-states. This is due to the large nuclear spin and nuclear magnetic moment of niobium.

In this work, the $4p^6n\ell$ spectrum of Nb V is extended to 84 lines and 30 levels using a sliding spark source. The Zeeman patterns of a few selected lines were examined using a modified sliding spark source. In addition, an attempt was made to study the ability of a laser to modify the population of energy levels in the sliding spark source.

II. THE EXPERIMENTAL APPARATUS

II.1. The Sliding Spark Source

II.1.1. Introduction

The idea of allowing a spark to slide along a surface dates back to 1867 when A. Toepler developed the sliding spark for schlieren photography. The uses of the source were mainly photographic until Vodar and Astoin [1950] studied the spectra from a sliding spark. They used a carbon rod as the spacer and copper rings for the electrodes. They easily discharged 30 kV across a gap of a few centimeters. Bockasten [1955] was the first to use a quartz spacer in his study of the third spectrum of carbon. Two French physicists did a large volume of work studying the spectra of many multiply charged ions, during which time they refined the sliding spark source to something very similar to the one we use (see Romand and Balloffet [1955] and Balloffet and Romand [1955] and [1956]). An excellent discussion of sliding spark sources, including a more detailed history, is contained in Beverly [1973].

In order to study the fifth spectrum of niobium, the sliding spark source was chosen for two reasons. The reason for using a spark source is that niobium is a metal that can conveniently be used as an electrode. The choice of the sliding spark source over the vacuum spark source was made because the current pulse shaping and pulse to pulse reproducibility needed to separate ion states are more easily achieved with the sliding spark source.

II.1.2. Pulse Shaping in the Sliding Spark Source

The shape and duration of the current pulse in the sliding spark source are controlled by placing the source in an LRC circuit as shown in Fig. II.1. The power supply charges the capacitor to the power supply voltage, V_o. The switch is an ignitron (Westinghouse model number: WL5550/681), which is fired by a thyratron (General Electric model number: FG-105), which is in turn fired by a TTL pulse. This switching system can, if desired, be replaced with a mechanical system using a rotating electrical contact. The switching was usually done at 1 to 10 times per second. When the switch is closed the energy stored in the capacitor is sent through the circuit. The inductance and resistance of this circuit can be varied in order to shape the resulting pulse. The resistor is a carbon stack, whose resistance can be varied slightly around the 1 to 2 ohm region. The inductor is just a set of coils of heavy copper wire which have inductances between 10 and 500 microhenries.

The mathematics of an LRC circuit are discussed in many texts (for example see Barger and Olsen [1973]. Briefly, the circuit equation is,

$$L \frac{d^2q}{dt^2} + R \frac{dq}{dt} + \frac{1}{C} q = 0$$

This may be rewritten as,

$$\frac{d^2q}{dt^2} + 2\gamma \frac{dq}{dt} + \omega_o^2 q = 0$$

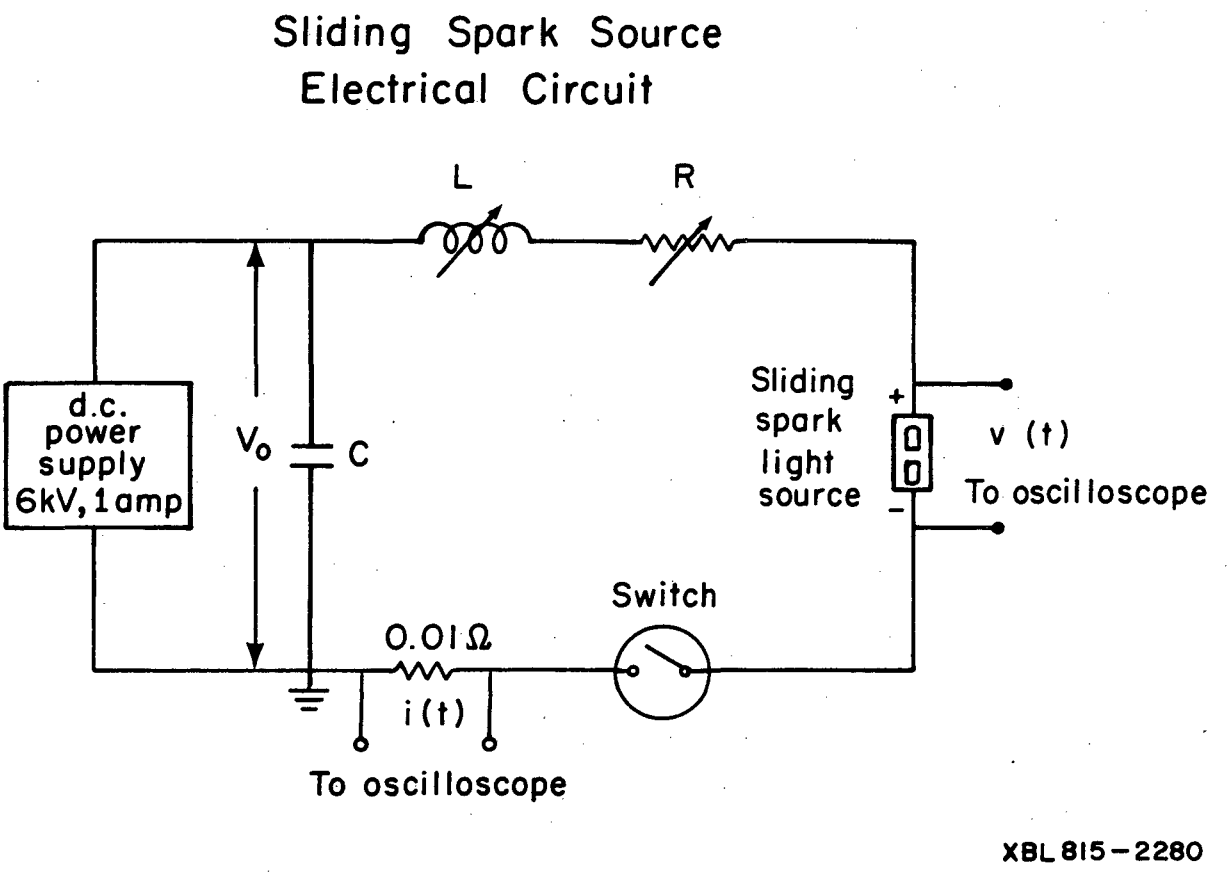

Figure II.1. Schematic of the sliding spark electrical circuit.

where,

$$\gamma = \frac{R}{2L} \qquad \text{and} \qquad \omega_o^2 = \frac{1}{LC}$$

Applying the initial conditions that,

$$q(t=0) = q_o = CV_o \qquad \text{and} \qquad i(t=0) = 0$$

one finds that the current as a function of time is given by,

$$i(t) = q_o \frac{\omega_o^2}{(\gamma^2-\omega_o^2)^{1/2}} \; e^{-\gamma t} \sinh (\gamma^2-\omega_o^2)^{1/2} t$$

In our source, the conditions are such that,

$$\gamma \simeq \omega_o$$

This is called 'critical damping' and results in a current pulse of the form,

$$i(t) = q_o \omega_o^2 t \; e^{-\omega_o t}$$

This analysis neglects the resistance of the spark which changes with time and makes the analytic solution of the circuit equation impossible. A more complete analysis of a sliding spark source can be found in a review article by Beverly [1978]. The particulars of our source are discussed by Van Deurzen [1973] and [1974]. The actual shape of a current pulse in our source is given in Figure II.2. Note that it is similar in appearance to the function i(t) given above for the case of critical damping. This function is also plotted in Figure II.2.

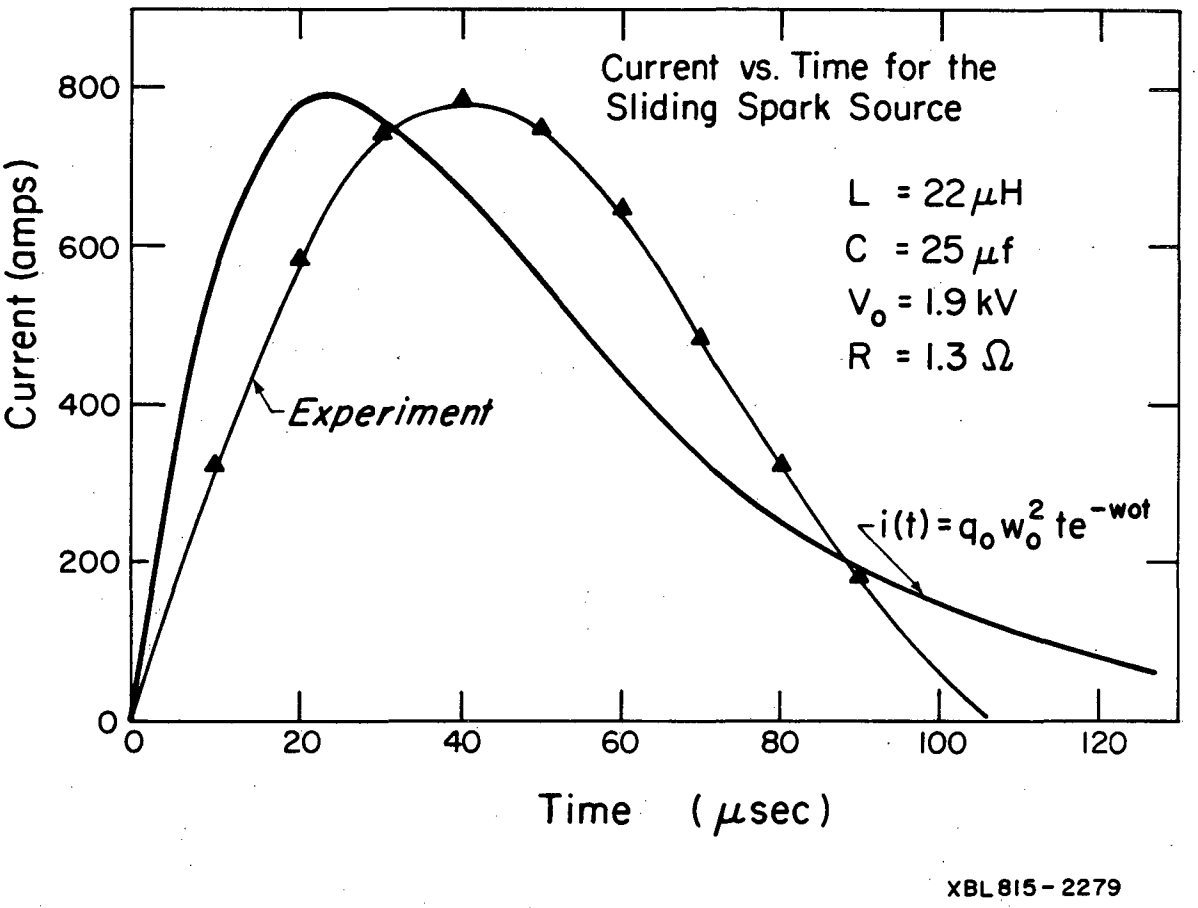

Figure II.2. Current as a function of time in the sliding spark source.

The ability to shape this current pulse can be seen by examining Table II.1. Notice that the duration of the pulse, as indicated by the full width at half maximum, can be varied from 50 microseconds to 1 millisecond, and the peak current can range from 30 amperes to 1200 amperes. The importance of this flexibility will be discussed later.

II.1.3. Details of the Light Source

Figure II.3a is a detailed drawing of the sliding spark source. Note that the niobium electrodes are separated by a quartz spacer along which the spark is allowed to slide. The electrodes are kept in place with copper holders which are connected to water cooled brass electrode mounts. Water flows through the source at about 5 to 10 gallons per minute. Even with this cooling, the spacer still glows red while the source is running at peak currents above 500 amps. The source is encased in glass and evacuated with a diffusion pump through a connection similar to the one in Figure II.3b. The electrical contacts at the top and bottom bring the current pulses into the source and the light pulses exit through the quartz window and are directed through some optics to the spectrograph.

II.1.4. Source Modifications for Zeeman Studies

Originally, the source designed by Lulu [1980] was used for the Zeeman studies. However, it proved inadequate at higher currents because it lacked a water cooling system. To facilitate the higher currents, a source as in Figure II.3a was constructed. However, it was

Table II.1. Circuit parameters for pulse shaping in the sliding spark source.

Inductance (uH)	V (Volts)	Current (Amps)	Full Width Half Max (usec)
593	1700	30	1000
593	1700	60	500
593	1700	100	320
312	1700	200	210
133	1600	300	140
68	1600	400	100
36	1500	600	80
11.5	1400	1000	60
0	1500	1200	48

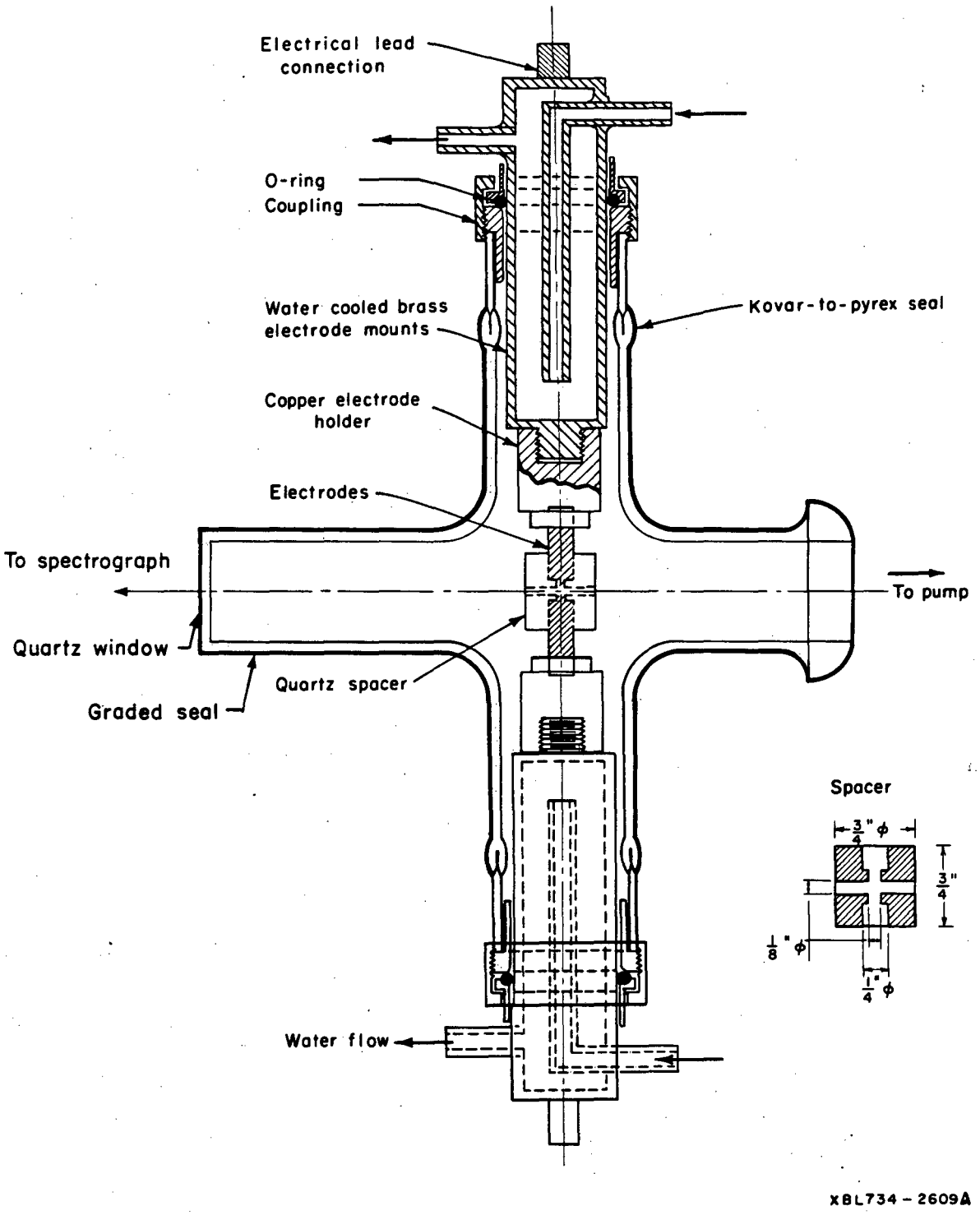

Figure II.3a. The sliding spark light source.

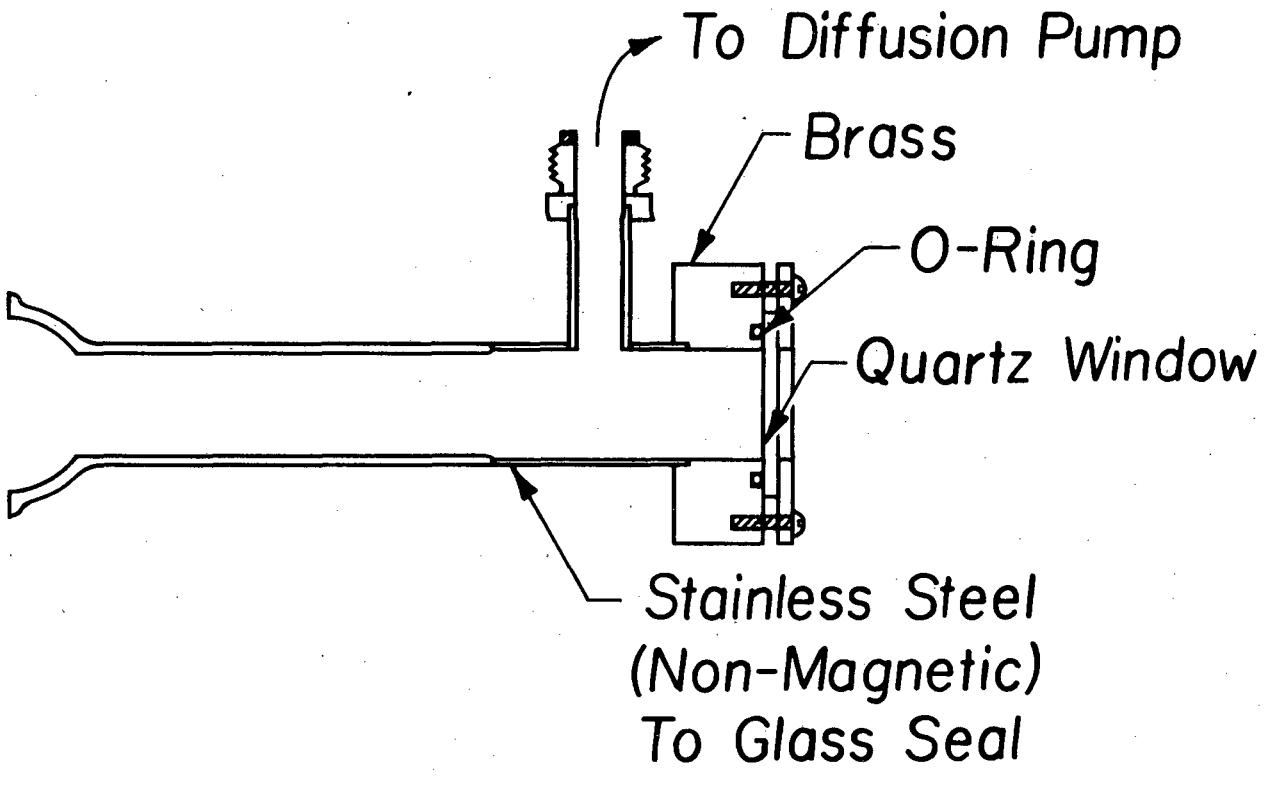

XBL 808-1821

Figure II.3b. The sliding spark light source.

scaled down to fit in the 2.86 cm gap between the poles of the magnet (see Figure II.4). In addition, the copper electrode holders had to be modified so that the electrodes could be held in such a way that the spark could travel along the field. They were designed so that the electrodes were parallel to each other, but separated by 3/32 of an inch, as in Figure II.5.

These modifications required changes in the spacer design. The first spacer that was tried was the simplest possible modification of the normal quartz spacer (see Figure II.5a). This spacer did not work mainly because the front viewing hole clogged up with the niobium that was sputtered off the electrodes in the violence of the spark in the magnetic field. In order to alleviate this problem and to confine the spark to a smaller path, a spacer as in Figure II.5b was made. It was constructed of lavite. Notice that the viewing port was quite larger and that the spark should be well confined along the back of the spacer.

II.1.5. Some Data on the Excitation of the Source

One might wonder, while examining the circuit diagram of Figure II.1, just how much energy actually gets to the sliding spark source. It appears that it might be a very small fraction of the energy stored in the capacitor, since after the spark starts, its resistance drops quickly. The one might be tempted to say that the energy of the capacitor would go toward heating the resistor. Trying analytically to solve this problem is quite difficult because one must suppose a model for the spark discharge. Instead of taking this approach, one can

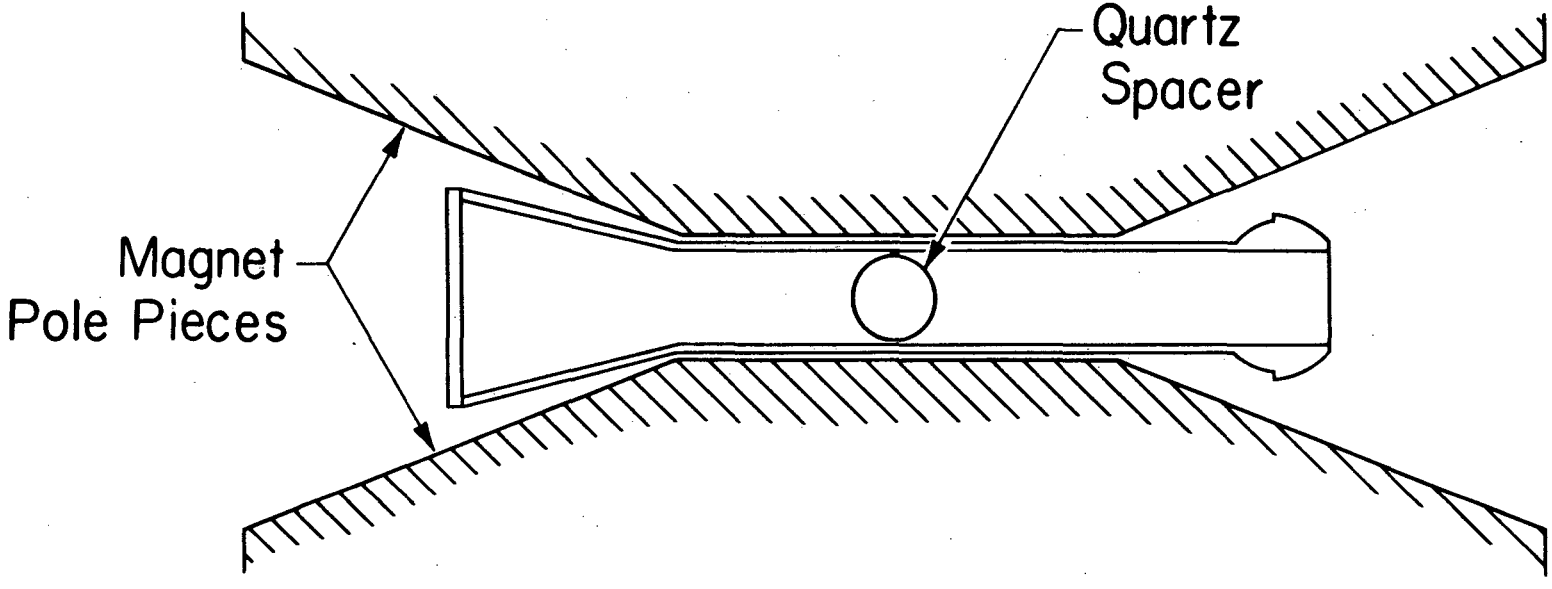

Figure II.4. The source in the magnet.

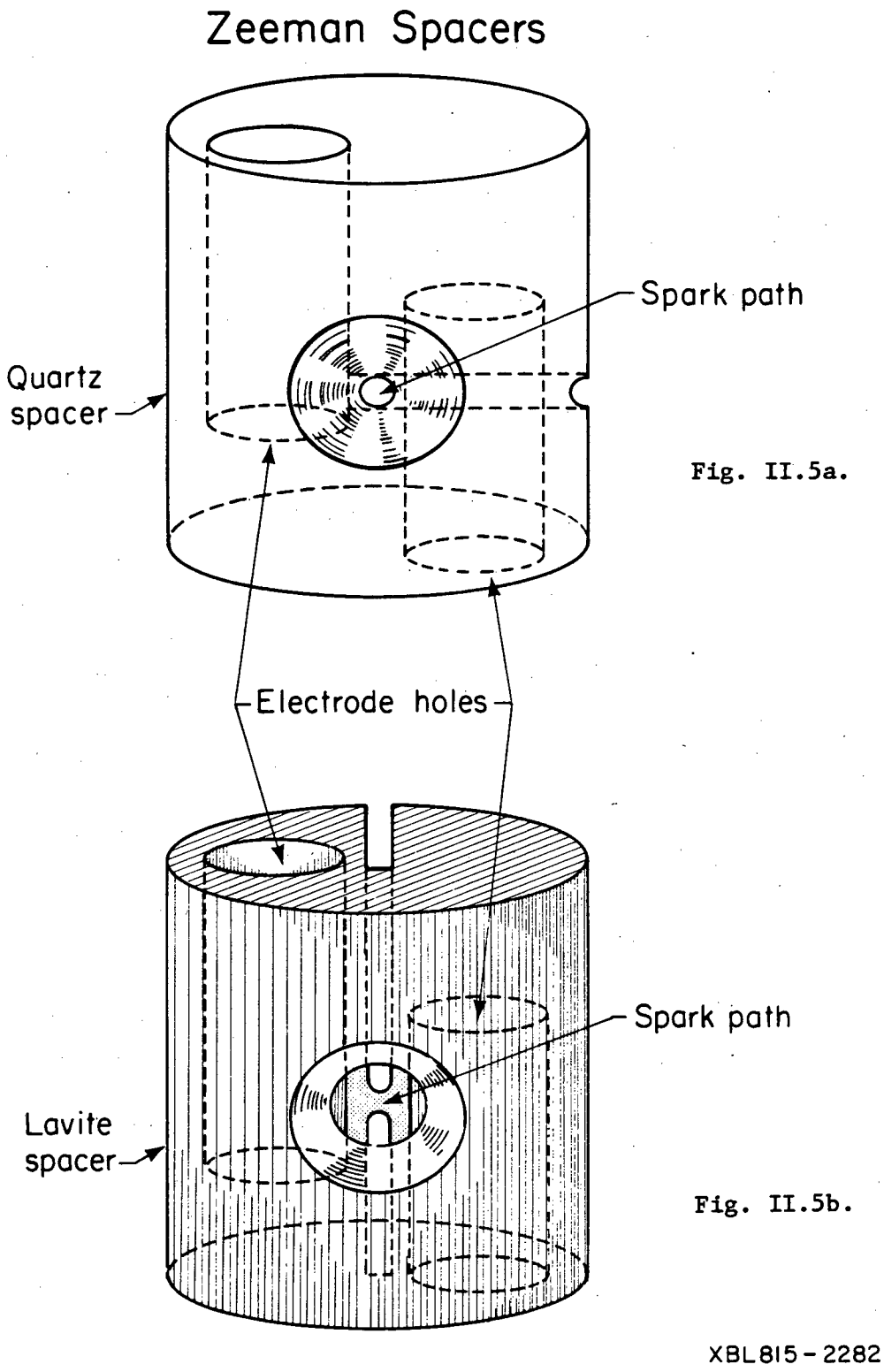

Fig. II.5a.

Fig. II.5b.

Figure II.5. The Zeeman spacers.

simply measure the current in the circuit, use that to find the ohmic losses in the resistor, and then substract this energy from the total to find the energy dumped into the source.

Table II.2 contains data taken with a typical set of circuit parameters. In a very crude fashion, one can find the total energy consumed in the resistor by the following formula,

$$E = R \sum_{n=1}^{9} \left| i_{n+1}^2 - i_n^2 \right| (t_{n+1} - t_n)$$

This is simply adding up the area of the trapazoids on the curve of power versus time. The result is about 30 joules. The energy originally stored on the capacitor is,

$$E = \frac{1}{2} CV_o^2$$

which is about 45 joules. The difference is 15 joules, so about one third of the total energy is dumped into the source. Unfortunately, not all of this energy manifests itself as light. The largest source of loss in the source is the generation of heat.

II.2. The Spectrographs and Plates

Three spectrographs were used for this experiment at Lawrence Berkeley Laboratory. In the far vacuum ultraviolet region a McPherson 247 2.2m grazing incidence was used (Figure II.6). In the near UV, a McPherson 241 3m normal incidence vacuum spectrograph was employed (Figure II.7). Finally, in the visible region, a Jarrell-Ash 3.4m Ebert

Table II.2. Current as a function of time in the sliding spark source.

Data Point n	Time (usec)	Current (amperes)
1	0	0
2	10	320
3	20	580
4	30	740
5	40	780
6	50	740
7	60	640
8	70	480
9	80	320
10	90	180

Circuit parameters: L = 22 uH
R = 1.3 ohms
C = 25 uf
V = 1.9 kV

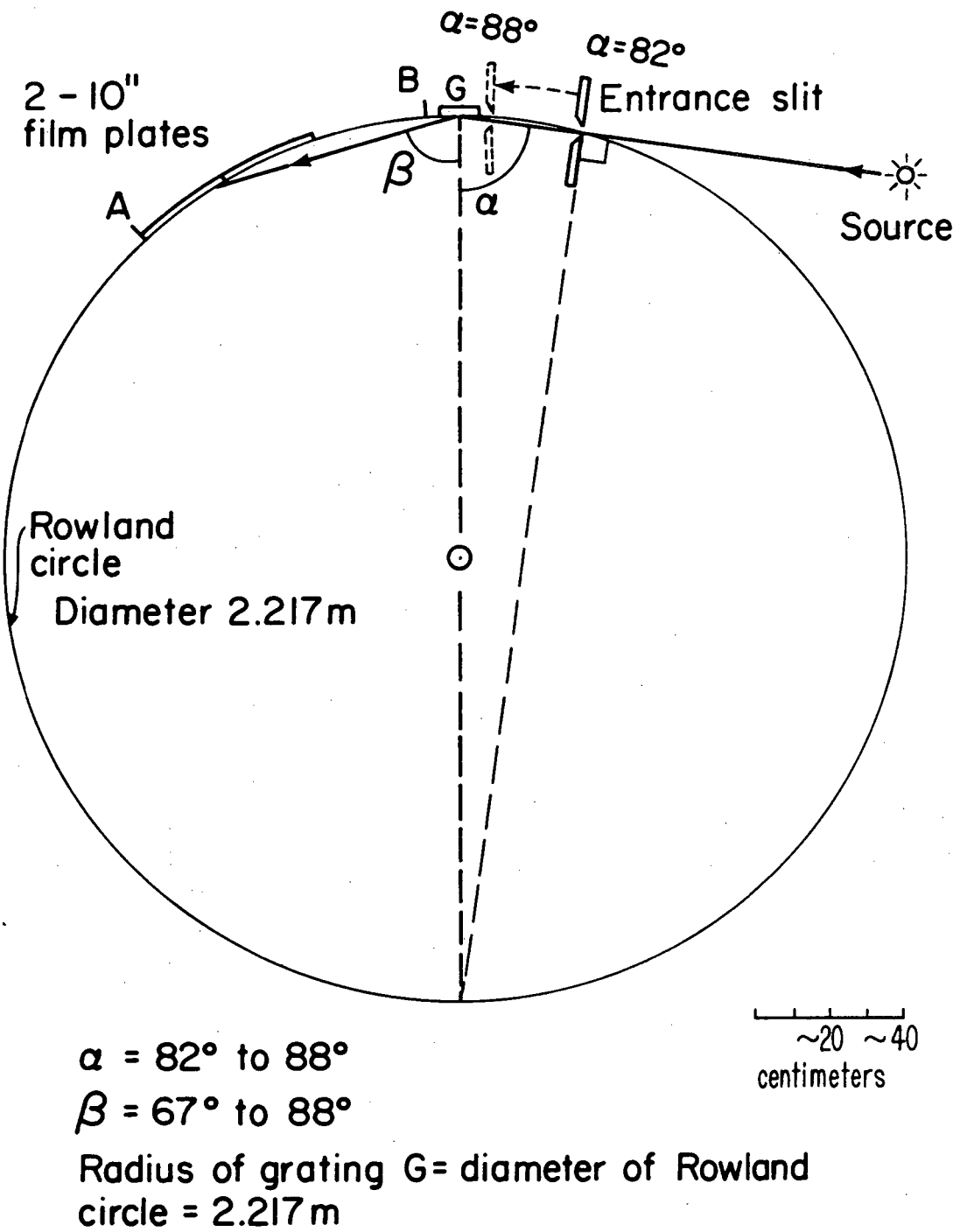

Figure II.6. McPherson 247 - 2.2m grazing incidence vacuum spectrograph.

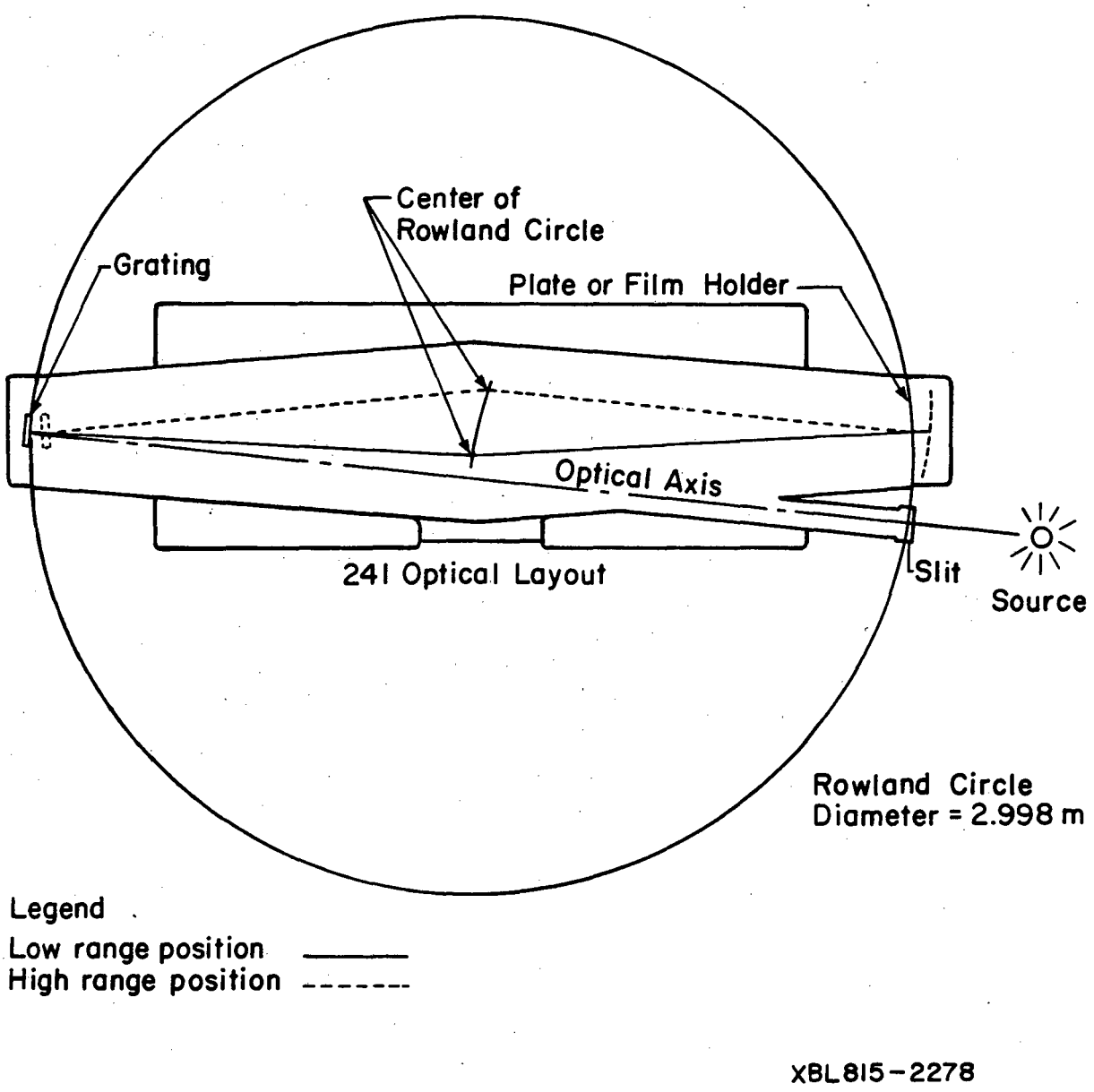

Figure II.7. McPherson 241- 3m normal incidence vacuum spectrograph.

spectrograph was used (Figure II.8). Table II.3 contains pertinent information on these three spectrographs including the types of spectroscopic plates there were used with each.

Since Dr. Erna Meinders of the Zeeman Laboratory in Amsterdam was also quite interested in the spectrum of Nb V, a collaboration was arranged. Dr. Meinders' spectrographs are also indicated in Table II.3. Notice that in the ultraviolet, the spectrographs at the Zeeman Laboratory have at least twice the plate factor. Therefore, wavelengths from Dr. Meinders were used whenever possible.

Developing of the Kodak 103a0 and 103aF plates was accomplished by placing the plates in Kodak D-19 developer for 3 minutes, followed by 30 seconds in a stop bath of weak acetic acid solution, then 3 minutes in Kodak Rapid Fixer. The plates were then washed in tap water for 10 to 15 minutes. The Kodak SWR plates were developed in the same fashion except that the D-19 developer was diluted to half strength.

The Kodak 10105 plates were much more difficult to develop properly. Before developing the plates they were allowed to soak in distilled water for about 10 minutes. Then they were placed in Kodak D-19 developer which was diluted with 3 parts distilled water to 1 part developer. The developer was kept at 55°F, and it was mildly agitated by hand as the plates developed. Since these plates weren't at all sensitive to red light, they were simply allowed to develop until the spectrum was visible. This usually took 2 to 3 minutes. The plates were then placed in the stop bath for 30 seconds, and then into the fixer for 2 to 3 minutes, followed by the usual 10 to 15 minute wash.

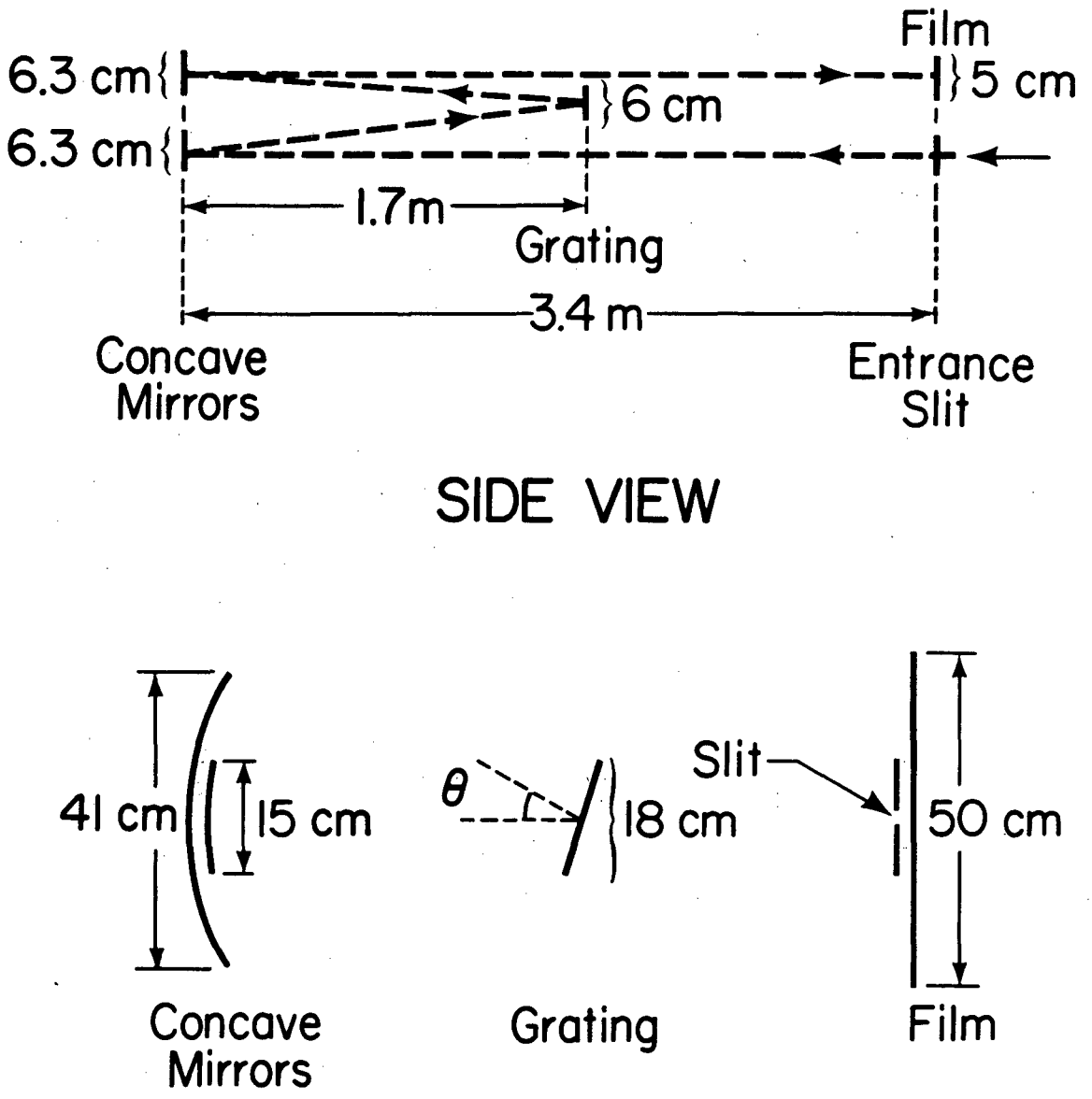

Figure II.8. Jarrell-Ash - 3.4m Ebert spectrograph.

Table II.3. Various data on the spectrographs.

	Location	Wavelengths (Angstroms)	Grating (lines/mm)	Plate Factor (Å/mm)	Plates	Standards
McPherson 247-2.2m Grazing Incidence Vacuum	LBL	200-700	1200	~1.0	Kodak 10105	SiIV, OIII, OIV
McPherson 241-3m Normal Incidence Vacuum	LBL	600-2800	1200	~2.8	Kodak SWR	CuII
Jarrell-Ash 3.4m Ebert	LBL	2500-4800	600	~5.0	Kodak 103a0	ThI, ThII
		4500-7000	600	~5.0	Kodak 103aF	ThI, ThII
		2500-4550	300	~0.5*	Kodak 103a0	ThI, ThII
6.65m Normal Incidence Vacuum	ZL	200-700	2400	~0.6	Kodak SWR	CuIII
		700-1250	2400	~0.6	Ilford Q2	CuII, CuIII
		1200-2300	1200	~1.2	Ilford Q2	CuII
Jarrell-Ash 3.4m Ebert	ZL	2000-2800	600	~2.5**	Ilford Q2	CuII

*12-23 order

**second order

For more detailed information on the plates, see Kodak Plates and Films for Scientific Photography [1973].

II.3. The Magnet

The magnet was a Spectromagnetic Industries electromagnet. It has a maximum field of about 28 kilogauss. The current was supplied by a model TC 200-300 power supply which is regulated to 0.01%. The pole pieces of the magnet are 10.16 cm in diameter and are separated by 2.86 cm. They are made of Permendur, which allows for higher fields then standard grade iron. A schematic of the magnet and power supply is given in Figure II.9. The magnetic field as a function of current is given in Table II.4, which is taken from Lulu [1980].

II.4. Wavelength Standards

The wavelength standards used for measuring the wavelengths of the Nb V lines varied depending on the region of the spectra studied. In the far vacuum ultraviolet region the only somewhat reliable standards were lines due to the materials in the spacer. Typically, these were silicon, oxygen, and carbon. The wavelengths of these lines are tabulated in Kelly and Palumbo [1973]. In the near vacuum ultraviolet, between 1000Å and 2800Å, a copper hallow cathode source was employed. Finally, from the ultraviolet to the infrared a thorium electrodeless lamp provided the standard lines. The wavelengths of these lines are found in Giacchetti et al. [1970].

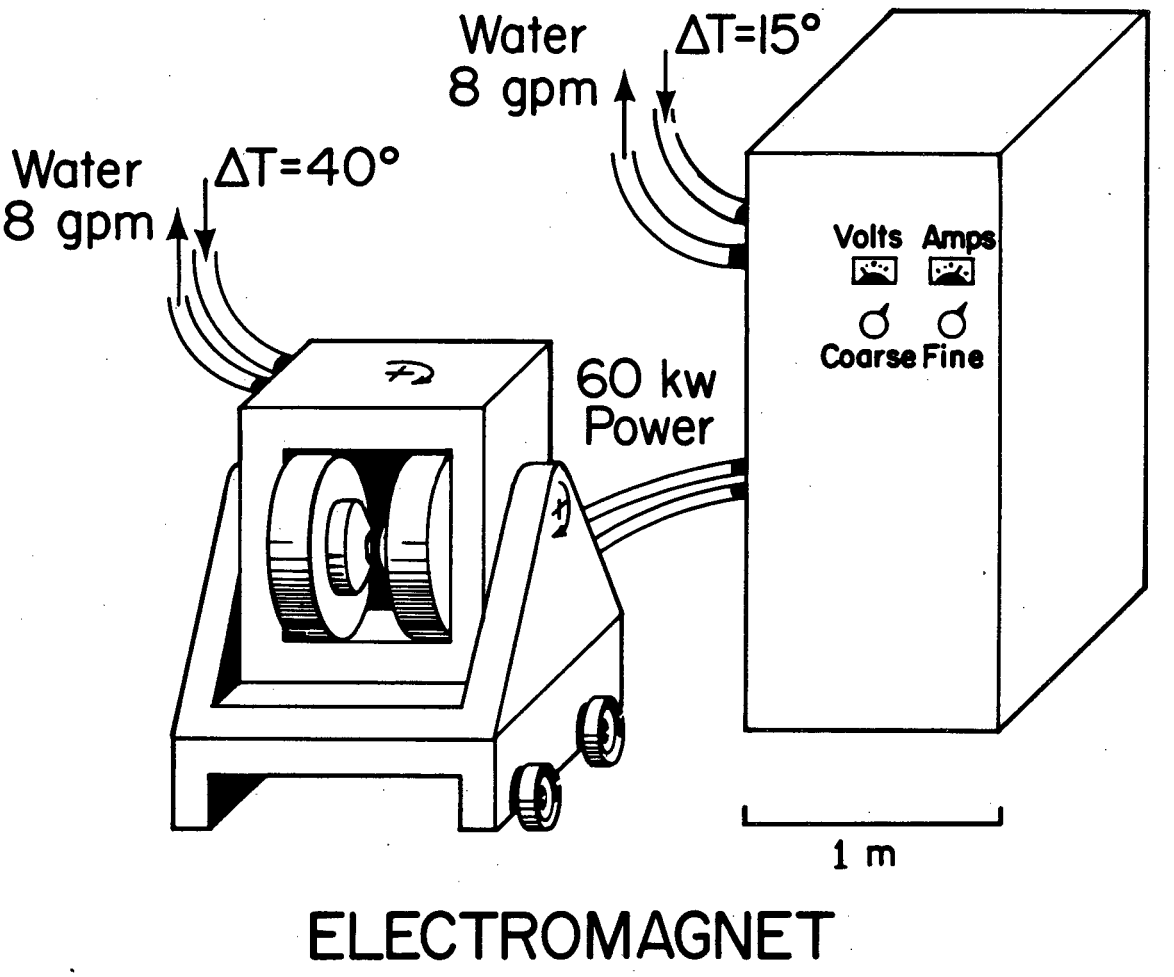

XBL 808-1813

Figure II.9. The magnet and its power supply.

Table II.4. Magnetic field vs. current for the magnet.

Current (amps)	Magnetic Field (gauss)
30	9518
60	18667
90	24042
120	25616
150	26313
180	26814
210	27243
240	27614
270	27950
300	28250

II.5. The Comparator

The plates were measured on a Grant Instruments Spectrum Line Measuring Comparator. This comparator has been modified so that computer cards containing the screw position of the lines are punched. These cards can then be turn into a wavelength list by the use of suitable CDC 7600 programs. This method of plate reading was used for the Nb V spectrum. In order to do the Zeeman studies, however, the comparator had to be modified a second time.

The Zeeman patterns of lines from a sliding spark source will not be resolved into individual lines due to Doppler broadening. To get a reasonable estimate of the g values of the lines, one must fit line profiles to overlapping gaussians. The easiest way to get line profile information from the comparator was to measure the darkening of the plate every micron or so. This was accomplished by using an LSI 11/2 mini-computer.

Figure II.10 is a block diagram of the Comparator Automation System (CAS). A optical encoder on the shaft of the comparator screw provided a sinusoidal signal which peaked every 2/1024 millimeters. This signal was amplified and used to fire a schmitt trigger which produced a TTL pulse to trigger the A/D converter on the LSI 11/2 computer. The A/D converter measured the signal from a phototube which was proportional to the transmission on the plate. These reading were stored on a floppy disc and could be recalled later for fitting the line profiles. A data point was taken every 1.953 microns. A 10 inch plate required 125,000

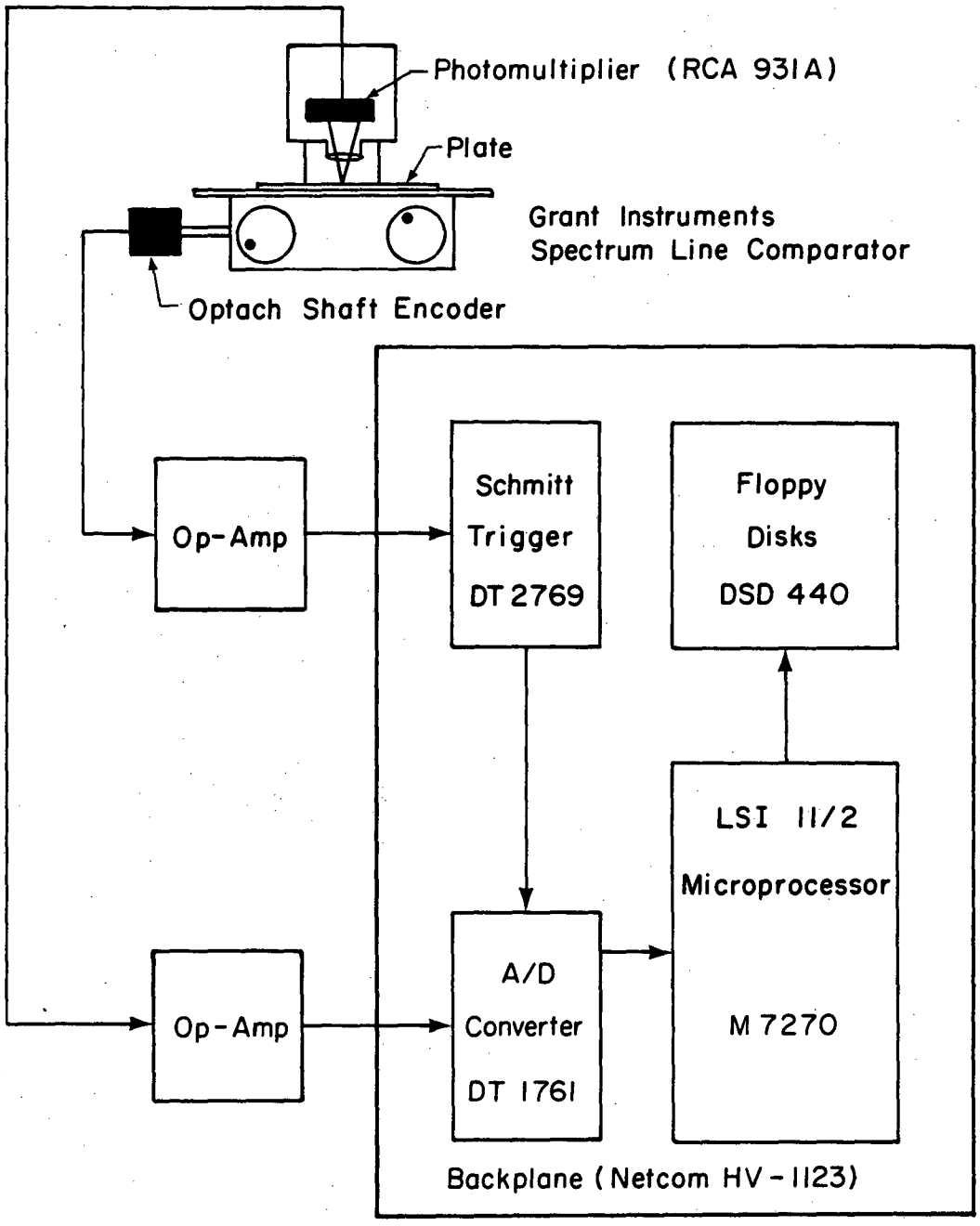

Figure II.10. The comparator automation system.

readings. The comparator moved at 2mm/sec or about a data point per millisecond. It took about 2 minutes to run an entire plate. Figures IV.3, IV.5, IV.7, IV.8 are samples of data taken by this method.

III. THE SPECTRUM OF FOUR-TIMES IONIZED NIOBIUM

III.1. Introduction

Four-times ionized niobium is isoelectronic with neutral rubidium. It has one electron outside of the krypton noble gas core. In many respects then, the spectrum is hydrogen-like. The first two members of the rubidium sequence, rubidium and strontium, have 5s ground states. However, the rest of the sequence, including niobium, have 4d ground states. Briefly, this is caused by fact that increasing nuclear charge contracts all of the orbits of the electrons, but the 5s, being a more penetrating orbit then the 4d, will feel more electron-electron repulsion and eventually have a higher energy then the 4d. A more complete discussion of this effect in the fourth period is contained in Griffin [1970].

The fifth spectrum of niobium was first investigated by Trawick in 1934. Trawick labeled 12 transitions in the UV, which established 10 energy levels. In 1950, G. W. Charles examined the Nb V spectrum. He found the weak components of the 4D - 4F transition that Trawick did not see and he established better wavelengths for the 4D - 4F and 4D - 5P transitions. Both of these works were done in conjunction with other rubidium-like spectra.

III.2. The Arc-to-Spark Method

As discussed earlier, the choice of the sliding spark source was made partly because this source offered the control of the shape and duration of the current pulse from an arc to a spark.

As one might suspect, in a long, low current, 'arc-like' discharge, only the lowest ionized species will occur. In a short, high current, 'spark-like' discharge, however, a greater number of higher charge state species will exist. If one takes a series of spectroscopic exposures, varying the current pulse from an arc to a spark, one should be able to see the onset of production of each charge state, its eventual predominance, and finally, its disappearance from the exposures.

Since the spectra of Nb I through Nb IV have been thoroughly studied (see Harrison [1939], Humphreys and Meggers [1945], Iglesias [1955], and Lang [1935]) and the spectra of Nb V and Nb VI have been partially examined (see Chaghtai [1969] and Reader, Epstein, and Ekberg [1972]), the behavior of each specie as the current is varied may be classified. In theory then, one has a method for determining the charge state of a given spectral line.

One problem that can occur is that impurities from the spacer may mimick the behavior of one or more of the niobium charge states. This problem may be overcome by the fact that most of the lines of the spacer impurities (oxygen, carbon, and silicon) are well known. These lines are tabulated by Kelly and Palumbo [1973].

This method of charge state assignment is discussed by Van Deurzen [1973].

III.3. Preparations

In order to have a serious chance of improving the Nb V spectrum, one must have at least some idea as to where to look for Nb V lines. This was done by estimating the energy of previously unseen levels. The first step was to plot the energy of the 6p ^2P and 5f ^2F levels of the rubidium isoelectronic sequence versus nuclear charge. The data for this plot was provided by Epstein and Reader [1975], Kiess [1956], Moore [1949], Romanov and Striganov [1969], and Evan-Zohar and Fraenkel [1972]. Interpolating this data gave estimates for the 6p ^2P and 5f ^2F levels in Nb V.

Combining these estimates with the known levels yields two levels for each angular momentum s, p, d, and f. Using quantum defect extrapolations, each angular momentum series could be extended to several terms. In addition, core-polarization calculations were used to get estimates of the levels in the ng ^2G, nh ^2H, and ni ^2I series. Both of these types of calculations are discussed by Edlén [1964]. Each time a new level was established by the data, these estimates were refined.

III.4. The Experiment and Its Results

The equipment discussed in Chapter II was used to take spectroscopic plates from the far ultraviolet to the near infrared. In each wavelength region two plates were taken. The first plate contained six tracks of niobium exposures at 60, 200, 300, 400, 600, and 1200 amperes, respectively. These current variation plates were used to separate charge

states as discussed in Section III.2. The second plate was used for measuring the wavelengths of the spectral lines. It contained a niobium track at 800 amperes and at least one standard track for calibration.

The current variation plates were scanned by eye for lines that behaved like the known lines of Nb V. These lines were not visible in the 60 amp track. They became barely visible in the 200 or 300 amp tracks and got increasingly stronger as the current was increased. Nearly all of these lines fit into the energy level scheme. They were classified and are listed in Table III.1. The wavelengths of lines that are less than 2000Å are given in vacuum, and the wavelengths of lines that are greater than 2000Å are given at 15°C and 760 Torr. The wavelengths that were contributed by Dr. Meinders are indicated by the initials 'em' in the wavenumber column.

The best values for the energy levels given by these assigned transitions were found by the least squares method. Briefly, this is done by finding the minimum of the residual given by,

$$R = \sum_{i=1}^{M} \sum_{j=1}^{N} \frac{n_{ij}}{(\Delta\sigma_{ij})^2} \left(E_i^{odd} - E_j^{even} - \sigma_{ij} \right)^2$$

E_i^{odd} and E_j^{even} are the energy levels involved in the transition of energy σ_{ij}. $\Delta\sigma_{ij}$ is the uncertainty in σ_{ij}, which is related to the relative weight that should be assigned to each transition. n_{ij} is either one or zero depending on whether the transition between i and j was observed or not. M is the number of odd levels and N is the number of even levels.

Table III.1. The classified lines of Nb V. The wavenumbers followed by em were from Meinders. The b in the intensity column means blend.

Assignment Odd		Even	Wavenumber (cm^{-1})	Wavelength* (Å)	Relative Intensity
$7p\ ^2P^o_{1/2}$	-	$6d\ ^2D_{3/2}$	18822.90	5311.200	50
$7p\ ^2P^o_{3/2}$	-	$7d\ ^2D_{3/2}$	18917.69	5284.587	10
$7p\ ^2P^o_{3/2}$	-	$7d\ ^2D_{5/2}$	19066.76	5243.270	70
$5f\ ^2F^o_{5/2}$	-	$5g\ ^2G$	19355.80	5164.971	40
$7p\ ^2P^o_{3/2}$	-	$6d\ ^2D_{5/2}$	19362.38	5163.216	60
$7p\ ^2P^o_{3/2}$	-	$6d\ ^2D_{3/2}$	19624.53	5094.243	10
$7p\ ^2P^o_{1/2}$	-	$7d\ ^2D_{3/2}$	19719.20	5069.786	40
$5f\ ^2F^o_{7/2}$	-	$5g\ ^2G$	19924.52	5017.542	70
$6h\ ^2H^o$	-	$7i\ ^2I$	20345.41	4913.741	100
$7h\ ^2H^o$	-	$6g\ ^2G$	20854.77	4793.725	100
$6p\ ^2P^o_{1/2}$	-	$6s\ ^2S_{1/2}$	22010.18	4542.078	90
$7p\ ^2P^o_{3/2}$	-	$8s\ ^2S_{1/2}$	23096.14	4328.510	40
$6p\ ^2P^o_{3/2}$	-	$6s\ ^2S_{1/2}$	23527.01	4249.237	100
$7p\ ^2P^o_{1/2}$	-	$8s\ ^2S_{1/2}$	23897.76	4183.313	20
$6f\ ^2F^o_{5/2}$	-	$5g\ ^2G$	24170.39	4136.127	30
$6f\ ^2F^o_{7/2}$	-	$5g\ ^2G$	25001.61	3998.611	40

*All wavelengths over 2000Å are given in air at 15°C and 760 Torr.

Table III.1. (continued).

Assignment Odd	Even	Wavenumber (cm^{-1})	Wavelength* (Å)	Relative Intensity
6f $^2F^o_{7/2}$	- 7g ^2G	29259.28	3416.74	20
6f $^2F^o_{5/2}$	- 7g ^2G	30090.98	3322.30	10
6f $^2F^o_{5/2}$	- 6d $^2D_{5/2}$	33837.8	2954.40	10
6f $^2F^o_{5/2}$	- 6d $^2D_{3/2}$	34100.64	2931.638	60
6h $^2H^o$	- 5g ^2G	34413.01	2905.026	100
6f $^2F^o_{7/2}$	- 6d $^2D_{5/2}$	34670.58	2883.444	90b
6p $^2P^o_{3/2}$	- 6d $^2D_{3/2}$	35140.21	2844.906	50
6p $^2P^o_{3/2}$	- 6d $^2D_{5/2}$	35402.38	2823.838	90
6p $^2P^o_{1/2}$	- 6d $^2D_{3/2}$	36657.09	2727.177	80
6p $^2P^o_{1/2}$	- 5d $^2D_{3/2}$	38812.56	2575.714	70
6p $^2P^o_{3/2}$	- 5d $^2D_{5/2}$	39784.94	2512.757	90
6p $^2P^o_{3/2}$	- 5d $^2D_{3/2}$	40328.9 em	2478.862	40
6p $^2P^o_{3/2}$	- 7s $^2S_{1/2}$	42712.7 em	2340.507	40
6p $^2P^o_{1/2}$	- 7s $^2S_{1/2}$	44229.5 em	2260.235	20
5p $^2P^o_{1/2}$	- 5s $^2S_{1/2}$	53265.7 em	1877.378	80
5p $^2P^o_{3/2}$	- 5s $^2S_{1/2}$	56870.1 em	1758.393	100

*All wavelengths over 2000Å are given in air at 15°C and 760 Torr.

Table III.1. (continued).

Assignment Odd	Assignment Even	Wavenumber (cm^{-1})	Wavelength (Å)	Relative Intensity
$5f\ ^2F^o_{5/2}$	$5d\ ^2D_{5/2}$	65496.5 em	1526.799	30b
$5f\ ^2F^o_{5/2}$	$5d\ ^2D_{3/2}$	66041.8 em	1514.193	40
$4f\ ^2F^o_{5/2}$	$6d\ ^2D_{3/2}$	71903.0	1390.76	10
$4f\ ^2F^o_{7/2}$	$6d\ ^2D_{5/2}$	72023.4	1388.44	40
$6p\ ^2P^o_{3/2}$	$7d\ ^2D_{5/2}$	73828.8	1354.49	20
$5f\ ^2F^o_{7/2}$	$7g\ ^2G$	74182.9	1348.02	10
$7p\ ^2P^o_{1/2}$	$6s\ ^2S_{1/2}$	77485.7	1290.56	3
$6p\ ^2P^o_{3/2}$	$8s\ ^2S_{1/2}$	77856.2	1284.42	6
$7p\ ^2P^o_{3/2}$	$6s\ ^2S_{1/2}$	78288.4	1277.33	6
$5p\ ^2P^o_{3/2}$	$5d\ ^2D_{3/2}$	78892.8 em	1267.543	50
$6p\ ^2P^o_{1/2}$	$8s\ ^2S_{1/2}$	79370.7	1259.91	3
$5p\ ^2P^o_{3/2}$	$5d\ ^2D_{5/2}$	79437.4 em	1258.853	90
$4f\ ^2F^o_{7/2}$	$5g\ ^2G$	81697.0 em	1224.035	70
$4f\ ^2F^o_{5/2}$	$5g\ ^2G$	81835.0 em	1221.971	60
$5p\ ^2P^o_{1/2}$	$5d\ ^2D_{3/2}$	82498.6 em	1212.142	80
$7p\ ^2P^o_{1/2}$	$5d\ ^2D_{3/2}$	94294	1060.51	15

Table III.1. (continued).

Assignment Odd	Even	Wavenumber (cm^{-1})	Wavelength (Å)	Relative Intensity
$7p\ ^2P^o_{3/2}$	$5d\ ^2D_{5/2}$	94548	1057.66	20
$5p\ ^2P^o_{3/2}$	$6s\ ^2S_{1/2}$	95696.1 em	1044.975	70
$5p\ ^2P^o_{1/2}$	$6s\ ^2S_{1/2}$	99301.6 em	1077.033	90b
$6f\ ^2F^o_{5/2}$	$5d\ ^2D_{5/2}$	109029	917.19	10
$6f\ ^2F^o_{5/2}$	$5d\ ^2D_{3/2}$	109569.7 em	912.661	20
$6f\ ^2F^o_{7/2}$	$5d\ ^2D_{5/2}$	109857.5 em	910.270	30
$4f\ ^2F^o_{7/2}$	$6g\ ^2G$	115520.1 em	865.650	10
$4f\ ^2F^o_{5/2}$	$6g\ ^2G$	115658.2 em	864.617	5
$5p\ ^2P^o_{1/2}$	$4d\ ^2D_{3/2}$	129195.0 em	774.024	90
$5p\ ^2P^o_{3/2}$	$4d\ ^2D_{5/2}$	130932.7 em	763.751	100
$5p\ ^2P^o_{3/2}$	$4d\ ^2D_{3/2}$	132800.2 em	753.011	70
$4f\ ^2F^o_{7/2}$	$7g\ ^2G$	135957.9 em	735.522	6
$4f\ ^2F^o_{5/2}$	$7g\ ^2G$	136097.6 em	734.767	3
$5p\ ^2P^o_{3/2}$	$6d\ ^2D_{3/2}$	154366.8 em	647.808	5
$5p\ ^2P^o_{3/2}$	$6d\ ^2D_{5/2}$	154627.4 em	646.716	20
$5p\ ^2P^o_{1/2}$	$6d\ ^2D_{3/2}$	157969.8 em	633.032	15

Table III.1. (continued).

Assignment Odd	Even	Wavenumber (cm^{-1})	Wavelength (Å)	Relative Intensity
$5p\ ^2P^o_{3/2}$	$7s\ ^2S_{1/2}$	161936.8 em	617.525	10
$5p\ ^2P^o_{1/2}$	$7s\ ^2S_{1/2}$	165541.1 em	604.080	5
$6p\ ^2P^o_{1/2}$	$5s\ ^2S_{1/2}$	174578 em	572.807	15
$6p\ ^2P^o_{3/2}$	$5s\ ^2S_{1/2}$	176094 em	567.879	20
$4f\ ^2F^o_{5/2}$	$4d\ ^2D_{5/2}$	213391 em	468.623	50
$4f\ ^2F^o_{7/2}$	$4d\ ^2D_{5/2}$	213530 em	468.318	100
$4f\ ^2F^o_{5/2}$	$4d\ ^2D_{3/2}$	215258 em	464.559	90
$6p\ ^2P^o_{3/2}$	$4d\ ^2D_{5/2}$	250157 em	399.749	50
$6p\ ^2P^o_{1/2}$	$4d\ ^2D_{3/2}$	250508 em	399.189	40
$6p\ ^2P^o_{3/2}$	$4d\ ^2D_{3/2}$	252024 em	396.788	20
$5f\ ^2F^o_{7/2}$	$4d\ ^2D_{5/2}$	275301 em	363.239	50
$5f\ ^2F^o_{5/2}$	$4d\ ^2D_{5/2}$	275871 em	362.488	20
$5f\ ^2F^o_{5/2}$	$4d\ ^2D_{3/2}$	277737 em	360.052	80b
$7p\ ^2P^o_{3/2}$	$4d\ ^2D_{5/2}$	304922	327.953	20
$7p\ ^2P^o_{1/2}$	$4d\ ^2D_{3/2}$	305989	326.809	10

Table III.1. (continued).

Assignment Odd	Even	Wavenumber (cm^{-1})	Wavelength (Å)	Relative Intensity
$7p\ ^2P^o_{3/2}$	$4d\ ^2D_{3/2}$	306794	325.952	1
$6f\ ^2F^o_{5/2}$	$4d\ ^2D_{3/2}$	319397	313.090	10
$6f\ ^2F^o_{7/2}$	$4d\ ^2D_{5/2}$	320222	312.283	50
$6f\ ^2F^o_{5/2}$	$4d\ ^2D_{5/2}$	321255	311.279	50

To minimize R, one must set its partial derivatives with respect to each energy level equal to zero.

$$\frac{\partial R}{\partial E_1^{odd}} = \frac{\partial R}{\partial E_2^{odd}} = \ldots = \frac{\partial R}{\partial E_M^{odd}} = \frac{\partial R}{\partial E_1^{even}} = \ldots = \frac{\partial R}{\partial E_N^{even}} = 0$$

This gives N+M equations of the form,

$$E_i^{odd} \sum_{j=1}^{N} \frac{n_{ij}}{(\Delta\sigma_{ij})^2} - \sum_{j=1}^{N} \frac{n_{ij}}{(\Delta\sigma_{ij})^2} E_j^{even} = \sum_{j=1}^{N} n_{ij} \frac{\sigma_{ij}}{(\Delta\sigma_{ij})^2}$$

$$i = 1,2,\ldots,M$$

$$\sum_{i=1}^{M} \frac{n_{ij}}{(\Delta\sigma_{ij})^2} E_i^{odd} - E_j^{even} \sum_{i=1}^{M} \frac{n_{ij}}{(\Delta\sigma_{ij})^2} = \sum_{i=1}^{M} n_{ij} \frac{\sigma_{ij}}{(\Delta\sigma_{ij})^2}$$

$$j = i,2,\ldots,N$$

These are then solved to give the least squares values for the N+M energy levels. The least squares fit levels are tabulated in Table III.2 and shown graphically in the Grotrian diagram Figure III.1. The residual deviation in the fit was 1.4 cm^{-1}, but this is mostly due to the large wavenumbers of most of the transitions. The least squares fit calculation of energy levels is thoroughly discussed by Radziemski [1970].

III.5. Some Analysis of the Data

III.5.1. The Ionization Energy

Using the series extrapolaton formulae of Edlén [1964], one can estimate the $4p^6\ {}^1S_0$ ionization limit. The first five entries in

Table III.2. The $4p^6n\ell$ levels of Nb V.

Level		Energy (cm^{-1})	Interval (cm^{-1})
$4d\ ^2D_{3/2}$		- 0 -	
$4d\ ^2D_{5/2}$		1867.4	1867.4
$5s\ ^2S_{1/2}$		75929.6	
$5p\ ^2P^o_{1/2}$		129195.2	
$5p\ ^2P^o_{3/2}$		132800.0	3604.8
$5d\ ^2D_{3/2}$		211694.0	
$5d\ ^2D_{5/2}$		212238.4	544.4
$4f\ ^2F^o_{5/2}$		215259.1	
$4f\ ^2F^o_{7/2}$		215397.5	138.4
$6s\ ^2S_{1/2}$	(F=4)	228495.7	
$6s\ ^2S_{1/2}$		228496.3	1.1
$6s\ ^2S_{1/2}$	(F=5)	228496.8	
$6p\ ^2P^o_{1/2}$		250506.5	
$6p\ ^2P^o_{3/2}$		252023.3	1516.8
$5f\ ^2F^o_{7/2}$		277169.7	
$5f\ ^2F^o_{5/2}$		277738.3	-568.6

Table III.2. (continued).

Level	Energy (cm^{-1})	Interval (cm^{-1})
6d $^2D_{3/2}$	287163.6	
		262.0
6d $^2D_{5/2}$	287425.6	
7s $^2S_{1/2}$	294736.0	
5g ^2G	297094.2	
7p $^2P^o_{1/2}$	305986.5	
		801.6
7p $^2P^o_{3/2}$	306788.1	
6f $^2F^o_{5/2}$	321264.4	
		831.5
6f $^2F^o_{7/2}$	322095.9	
7d $^2D_{3/2}$	325705.7	149.1
7d $^2D_{5/2}$	325854.8	
8s $^2S_{1/2}$	329884.2	
6g ^2G	330917.5	
6h $^2H^o$	331507.2	
7g ^2G	351355.3	
7h $^2H^o$	351772.2	
7i ^2I	351852.6	

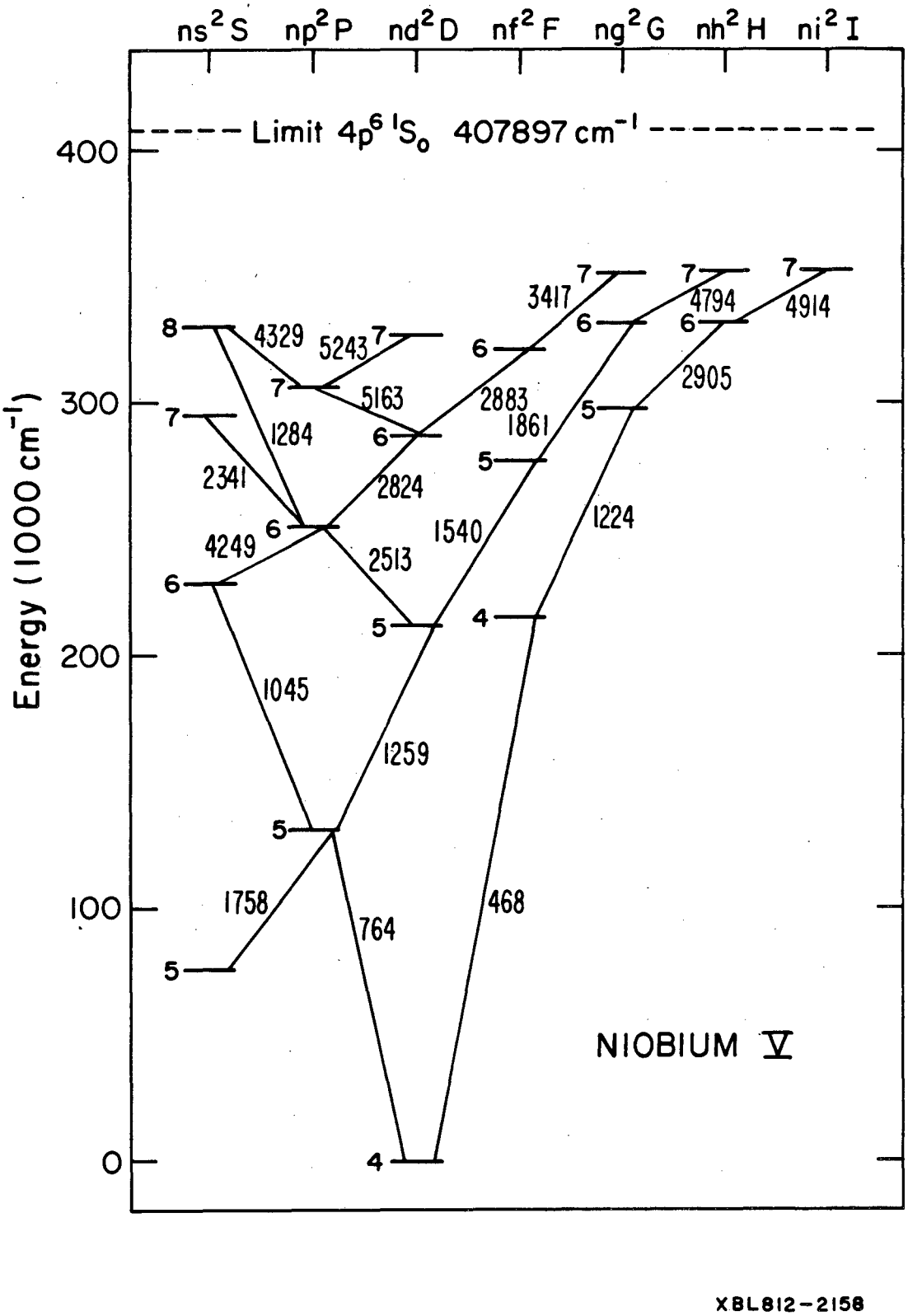

Figure III.1. The Grotrian diagram for Nb V.

Table III.3 are the values of these estimates for each angular momentum. The quality of these estimates depends upon the amount of interaction with the electron core and the possible mixing of states from the configuration interaction. The worst estimate comes from the f series. This poor value indicates that this series is indeed perturbed by another configuration.

The last two entries in Table III.3 were calculated by using a core-polarization model also discussed by Edlén [1964]. Since the interaction between the core and these high angular momentum states is very well represented by the polarization of the core, the resulting values of the ionization energy are considered the best. The best value for the $4p^6\ {}^1S_0$ ionization limit is then 407897 cm^{-1}. The error in this value is difficult to estimate, but it is certainly not larger than 40 cm^{-1}.

III.5.2. Perturbations and Configuration Mixing

As mentioned above, the $4p^6nf$ series yields an anomalously large value of the $4p^6\ {}^1S_0$ ionization energy. In addition, the fine-structure interval of the 4f, 5f, and 6f levels do not follow the typical decrease in size with increasing n. In fact, the 5f level is inverted and the 6f level has a larger fine-structure than the 4f. All of these facts point to a configuration interaction between the $4p^6nf$ levels and another configuration.

Table III.3. Estimates of the ionization energy of Nb V.

Levels used for calculation	Ionization Energy (cm^{-1})
6s, 7s, 8s	407613
5p, 6p, 7p	407469
5d, 6d, 7d	407554
4f, 5f, 6f	431515
5g, 6g, 7g	407863
6h, 7h, 7i	407886*
5g, 6g, 7g, 6h, 7h, 7i	407897*

*Calculated by the core polarization method, all others found from quantum defect extrapolation.

Since configuration mixing only occurs between states of the same parity and roughly the same energy, the likely candidates for the perturbing level or levels are $4p^5 4d^2$, and $4p^5 5s 4d$, and $4p^5 5s^2$. The large effective charge of four-times ionized niobium would tend to try and order the energy of the levels in a hydrogenic way. That is to say, the lowest levels having the lowest values of n. One might guess then, that the $4p^5 4d^2$ levels are the ones that provide the strongest mixing. This guess is somewhat substantiated by Mushtaq [1979] who found that the lowest level of the $4p^5 5s 4d$ configuration is at 345201 cm^{-1}, which is well above the $4p^6 5f$ level. Also, Van Deurzen [1977] found that the $3p^5 3d^2$ levels of four-times ionizied vanadium (ground state $3p^6 3d$) to be more than 100,000 cm^{-1} lower in energy than the $3p^5 4s 3d$ levels.

III.5.3. The Hyperfine Splitting of the S-States

In Table III.2, the hyperfine splitting of the $4p^6 6s$ level is indicated. This splitting was seen in the 6p ^2P to 6s ^2S transitions in the visible (4249.237 Å and 4542.078 Å). The splitting was visible on these plates because the dispersion was quite large (the plate factor was 0.5 angstroms per millimeter). Meinders observed the hyperfine splitting of the $4p^6 5s$ level in the 5p ^2P to 5s ^2S transitions at 1877.378 Å and 1758.383 Å. She was unable to measure the splitting because the components weren't resolved, but she estimated the splitting to be about 2 cm^{-1}.

IV. THE ZEEMAN EFFECT OF SELECTED Nb V LINES

IV.1. Introduction

In 1896, Peder Zeeman [1897] found that if a sodium flame was placed between the poles of an electromagnet, the spectral lines of the flame were split. This was interpreted by H. A. Lorentz in terms of classical orbits of a charged particle. The charge to mass ratio of this particle was identical to the one discovered by Thompson at about the same time. This particle is of course, the electron. Lorentz predicted that the light viewed perpendicular to the field would split into three lines, the center of which would be polarized along the field direction and the outer two would be polarized perpendicular to the field. These predictions were later verified by Zeeman himself.

It was not long before Preston [1898] found that the Zeeman patterns were not always composed of three lines. This was the first evidence of the "anomalous" Zeeman effect, which was not explained until Uhlenbeck and Goudsmit [1925] proposed the existence of the intrinsic angular momentum of the electron.

Since the turn of the century then, people have been using the Zeeman effect as a spectroscopic tool. However, to the author's knowledge, no one has examined the Zeeman spectra of a four-times ionized specie. The reason for this is that sources that have enough energy to create four-times ionized ions have Doppler widths that are larger than the Zeeman splitting. Indeed, this is a problem that had to be dealt with.

IV.2. The Theory of the Zeeman Effect

IV.2.1. The Zeeman Hamiltonian

The Hamiltonian for an N-electron atom contains many terms, but the one of interest for the Zeeman effect is the kinetic energy term. One can represent the Hamiltonian as,

$$H_0 = \sum_{j=1}^{N} \frac{(\vec{\sigma}_j \cdot \vec{p}_j)(\vec{\sigma}_j \cdot \vec{p}_j)}{2m} + \text{other terms}$$

Where $\vec{p}_j$ is the momentum of the jth electron, m is the electron mass, $\vec{\sigma}$ are the Pauli spin matrices, and "other terms" represents all of the other interactions, such as the Coulomb interaction with the nucleus and the other electrons, as well as the spin-orbit interaction, and possibly even spin-spin interactions. The standard method for modifying the Hamiltonian to account for external electromagnetic fields is to perform the following replacement:

$$\vec{p}_j \rightarrow \vec{p}_j + \frac{e}{c} \vec{A}(\vec{r}_j)$$

where e is the absolute value of the charge of the electron, c is the speed of light, and $\vec{A}(\vec{r}_j)$ is the vector potential. The new Hamiltonian is then,

$$H = H_0 + \frac{e}{2mc} \sum_{j=1}^{N} \left\{ (\vec{\sigma}_j \cdot \vec{p}_j)(\vec{\sigma}_j \cdot \vec{A}(\vec{r}_j)) + (\vec{\sigma}_j \cdot \vec{A}(\vec{r}_j))(\vec{\sigma}_j \cdot \vec{p}_j) \right\}$$

$$+ \frac{e^2}{2mc^2} \sum_{j=1}^{N} (\vec{\sigma}_j \cdot \vec{A}(\vec{r}_j))^2$$

Using the fact that all the Pauli matrices commute with all of the components of momentum and all the components of the vector potential, as well as the relations,

$$\sigma_x\sigma_x = 1 \qquad \sigma_y\sigma_x = -i\sigma_z \qquad \sigma_z\sigma_x = i\sigma_y$$
$$\sigma_x\sigma_y = i\sigma_z \qquad \sigma_y\sigma_y = 1 \qquad \sigma_z\sigma_y = -i\sigma_x$$
$$\sigma_x\sigma_z = -i\sigma_y \qquad \sigma_y\sigma_z = i\sigma_x \qquad \sigma_z\sigma_z = 1$$

One can rewrite the Hamiltonian as,

$$H = H_0 + \frac{e}{2mc} \sum_{j=1}^{N} \left\{ (\vec{p}_j \cdot \vec{A}(\vec{r}_j)) + (\vec{A}(\vec{r}_j) \cdot \vec{p}_j) + i\vec{\sigma}_j \cdot (\vec{p}_j \times \vec{A}(\vec{r}_j)) \right.$$
$$\left. + i\vec{\sigma}_j \cdot (\vec{A}(\vec{r}_j) \times \vec{p}_j) \right\} + \frac{e^2}{2mc^2} \sum_{j=1}^{N} (\vec{A}(\vec{r}_j))^2$$

In the Coulomb gauge the divergence of the vector potential is zero. Therefore,

$$\vec{p}_j \cdot \vec{A}(\vec{r}_j) = \vec{A}(\vec{r}_j) \cdot \vec{p}_j$$

Also, careful inspection of the operators $\vec{p}_j$ and $\vec{A}(\vec{r}_j)$ reveals,

$$\vec{\sigma}_j \cdot \{ (\vec{p}_j \times \vec{A}(\vec{r}_j)) + (\vec{A}(\vec{r}_j) \times \vec{p}_j) \} = \vec{\sigma}_j \cdot (\vec{p}_j \times \vec{A}(\vec{r}_j))$$

Yielding the Hamiltonian,

$$H = H_0 + \frac{e}{mc} \sum_{j=1}^{N} (\vec{A}(\vec{r}_j) \cdot \vec{p}_j) + \frac{ie}{2mc} \sum_{j=1}^{N} \vec{\sigma}_j \cdot (\vec{p}_j \times \vec{A}(\vec{r}_j))$$
$$+ \frac{e^2}{2mc^2} \sum_{j=1}^{N} (\vec{A}(\vec{r}_j))^2$$

In the Zeeman effect one has a static, homogeneous magnetic field, B, which is the result of a vector potential of the form,

$$\vec{A}(\vec{r}_j) = \frac{1}{2} \vec{B} \times \vec{r}_j$$

Using the definitions,

$$\vec{L}_j = \vec{r}_j \times \vec{p}_j \qquad \vec{S}_j = \frac{\hbar}{2} \vec{\sigma}_j \quad \text{and} \quad \vec{B} = \nabla \times \vec{A}$$

H now becomes,

$$H = H_o + \frac{e}{2mc} \sum_{j=1}^{N} \vec{L}_j \cdot \vec{B} + \frac{e}{mc} \sum_{j=1}^{N} \vec{S}_j \cdot \vec{B} + \frac{e^2}{2mc^2} \sum_{j=1}^{N} (\vec{A}(\vec{r}_j))^2$$

For field strengths of interest here, the last term is negligible. Using the following definitions,

$$\vec{L} = \sum_{j=1}^{N} \vec{L}_j \qquad \vec{S} = \sum_{j=1}^{N} \vec{S}_j \qquad \vec{J} = \vec{L} + \vec{S}$$

and allowing the magnetic field to define the z-axis, one finally obtains the Zeeman Hamiltonian,

$$H = H_o + \frac{eB}{2mc} (J_z + S_z)$$

IV.2.2. The Zeeman Energy Levels and Wavefunctions

The energy levels for the Zeeman Hamiltonian can be found by first order perturbation theory. Using basis states of the form,

$$|n,\ell,s,j,m_j\rangle$$

one finds the energy shifts to be,

$$\Delta E = \frac{eB}{2mc}\{\langle n,\ell,s,j,m_j|J_z|n,\ell,s,j,m_j\rangle + \langle n,\ell,s,j,m_j|S_z|n,\ell,s,j,m_j\rangle\}$$

$$\Delta E = \frac{eB}{2mc}\{m_j\hbar + \langle n,\ell,s,j,m_j|S_z|n,\ell,s,j,m_j\rangle\}$$

The matrix element of S_z can be evaluated by using the Wigner-Eckart theorem. Now one arrives at the well known result,

$$\Delta E = \frac{e\hbar B}{2mc}\, m_j g_j \quad \text{where} \quad g_j = \begin{cases} 0 & j=0 \\ 1 + \dfrac{j(j+1)+s(s+1)-\ell(\ell+1)}{2j(j+1)} & j\neq 0 \end{cases}$$

The quantity g_j is known as the Landé g-factor. Notice that each energy level in the zero field case is split into 2j+1 evenly spaced levels, and that this removes all the degeneracy in the zero field levels. The energy shift can be rewritten as,

$$\Delta E = \mu_B B m_j g_j$$

where μ_B is the Bohr magneton given by,

$$\mu_B = \frac{e\hbar}{2mc}$$

In this experiment the magnetic field was measured to be 27.62 kilogauss. The energy shifts are given by,

$$\Delta E = (1.289\ \text{cm}^{-1}) m_j g_j$$

The first order corrected wavefunctions are given by,

$$|\text{new}\rangle = |n,\ell,s,j,m_j\rangle + \sum' \frac{\langle n,\ell,s,j,m_j|H|n',\ell',s',j',m_j'\rangle}{E - E'} |n',\ell',s',j',m_j'\rangle$$

Since the Zeeman Hamiltonian commutes with L, S, and J_z, the only states that mix are ones that have the same ℓ, s, and m_j, but different j. The mixing of such states is proportional to the ratio of the Zeeman energy shift to the difference of the energy of the mixing states. The smallest value of this energy difference is the fine-structure interval which in most cases is much greater than the Zeeman energy. For these cases the wavefunctions are only slightly mixed by the magnetic field, and will be considered unmixed for the remainder of Section IV.2.

IV.2.3. Transitions - Selections Rules, Polarization, and Intensities

The transition probability per unit time for dipole transitions between the states $|n,\ell,s,j,m_j\rangle$ and $|n',\ell',s',j',m_j'\rangle$ is shown by Sakurai [1967] to be proportional to,

$$W = \langle n,\ell,s,j,m_j|\vec{r}|n',\ell',s',j',m_j'\rangle\cdot\hat{\varepsilon}$$

where $\hat{\varepsilon}$ is the polarization direction of the emitted light. Since $\vec{r}$ is a spherical tensor operator, the Wigner-Eckart theorem may be used to find the selection rules for the allowed dipole transitions. These selection rules are,

$$\Delta j = 0, \pm 1 \quad \text{and} \quad \Delta m_j = 0, \pm 1$$

In addition, $\vec{r}$ is of odd parity. Thus, only states of opposite parity may undergo dipole transitions. In the case of the $4p^6n\ell$ spectrum of Nb V, this means that,

$$\Delta\ell = \pm 1$$

The polarization of the emitted light may be found by using the Wigner-Eckart theorem to evaluate the transition probability. These results are given by Condon and Shortley [1970],

$$M_1 = \langle n,\ell,s,j,m_j|\vec{r}|n',\ell',s',j+1,m_j\pm 1\rangle$$

$$= \mp \langle n,\ell,s,j\|r\|n',\ell',s',j+1\rangle \frac{1}{2}\sqrt{(j\pm m_j+1)(j\pm m_j+2)}\ (\hat{x}\pm i\hat{y})$$

$$M_2 = \langle n,\ell,s,j,m_j|\vec{r}|n',\ell',s',j+1,m_j\rangle$$

$$= \langle n,\ell,s,j\|r\|n',\ell',s',j+1\rangle \sqrt{(j+1)^2-m_j^2}\ \hat{z}$$

$$M_3 = \langle n,\ell,s,j,m_j|\vec{r}|n',\ell',s',j,m_j\pm 1\rangle$$

$$= \langle n,\ell,s,j\|r\|n',\ell',s',j\rangle \frac{1}{2}\sqrt{(j\mp m_j)(j\pm m_j+1)}\ (\hat{x}\pm i\hat{y})$$

$$M_4 = \langle n,\ell,s,j,m_j|\vec{r}|n',\ell',s',j,m_j\rangle$$

$$= \langle n,\ell,s,j\|r\|n',\ell',s',j\rangle\ m_j\hat{z}$$

$$M_5 = \langle n,\ell,s,j,m_j|\vec{r}|n',\ell',s',j-1,m_j\pm1\rangle$$

$$= \pm\langle n,\ell,s,j\|r\|n',\ell',s',j-1\rangle \frac{1}{2}\sqrt{(j\mp m_j)(j\mp m_j-1)}\ (\hat{x}\pm i\hat{y})$$

$$M_6 = \langle n,\ell,s,j,m_j|\vec{r}|n',\ell',s',j-1,m_j\rangle$$

$$= \langle n,\ell,s,j\|r\|n',\ell',s',j-1\rangle \sqrt{j^2-m_j^2}\ \hat{z}$$

Consider the geometry of the experiment, which is indicated in Fig. IV.1. The magnetic field defines the z-axis. If one then defines the viewing axis as the y-axis, then the light that one sees is either polarized along the x-axis or along the z-axis. Light that is polarized along the z-axis, parallel to the field, is said to be π-polarized, and light that is polarized along the x-axis, perpendicular to the field, is σ-polarized. For the π-polarized light, the transition probability is related to,

$$W_\pi = \langle n,\ell,s,j,m_j|\vec{r}|n',\ell',s',j',m_j'\rangle \cdot \hat{z}$$

Only the matrix elements, M_2, M_4, and M_6 have z components. Thus, the π-polarized light is only from transitions in which $\Delta m_j = 0$.

For the σ-polarized light, one has,

$$W_\sigma = \langle n,\ell,s,j,m_j|\vec{r}|n',\ell',s',j',m_j'\rangle \cdot \hat{x}$$

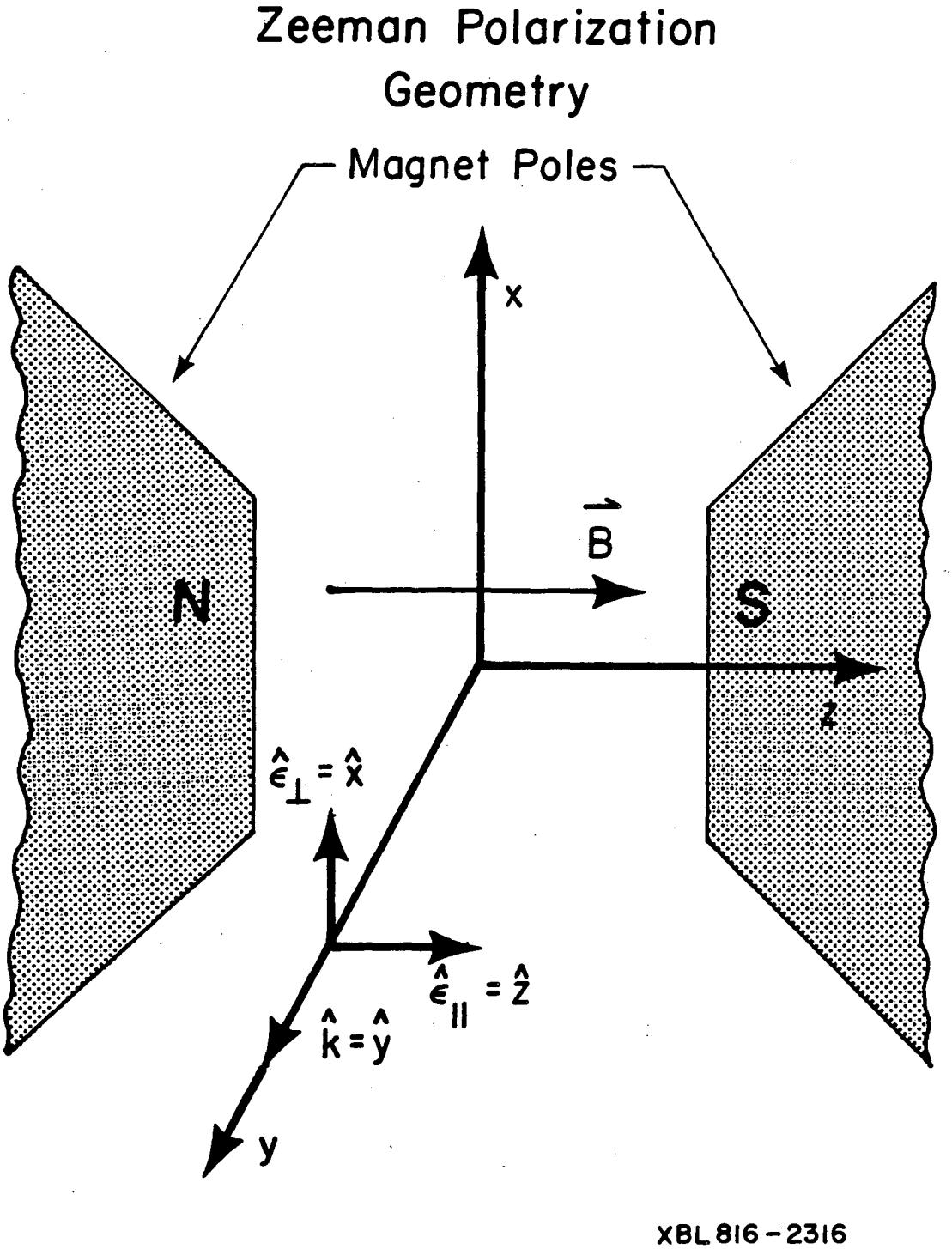

Figure IV.1. Zeeman polarization geometry.

The matrix elements M_1, M_3, and M_5 are the only ones that have x components. This means that σ-polarized light is from transitions where $\Delta m_j = \pm 1$.

The intensity of the transitions between states is proportional to,

$$I = |W|^2$$

If one examines the Zeeman pattern which contains the collection of transitions from the states with $j=j_1$ to the states with $j=j_2$, the relative intensity of the various transitions can be found because the matrix elements on the right hand side of the M's above, depend only on the n's, ℓ's, s's, and j's, and definitely not on the m_j's (that is the point of the Wigner-Eckart theorem).

Figure IV.2 is an example of the results of this section. The transition involved is the 6p $^2P_{3/2}$ to 5d $^2P_{5/2}$. Notice that the splitting of the $^2P_{3/2}$ levels is different than the splitting between the $^2D_{5/2}$ levels. This is due to the difference in g-values for the two levels. The result of this difference is that the collection of transitions involving a given value of Δm_j(-1,0, or +1) are separated in energy by the difference in the g-values times $\mu_B B$. This separation is known as the 'anomalous' Zeeman effect. This anomalous structure was not seen in this experiment because of the Doppler width of the spectral lines. The relative intensities of the various components of the Zeeman pattern, as well as their relative separation are indicated at the bottom of the Figure IV.2. The upper lines are π-polarized and the lower ones are σ-polarized.

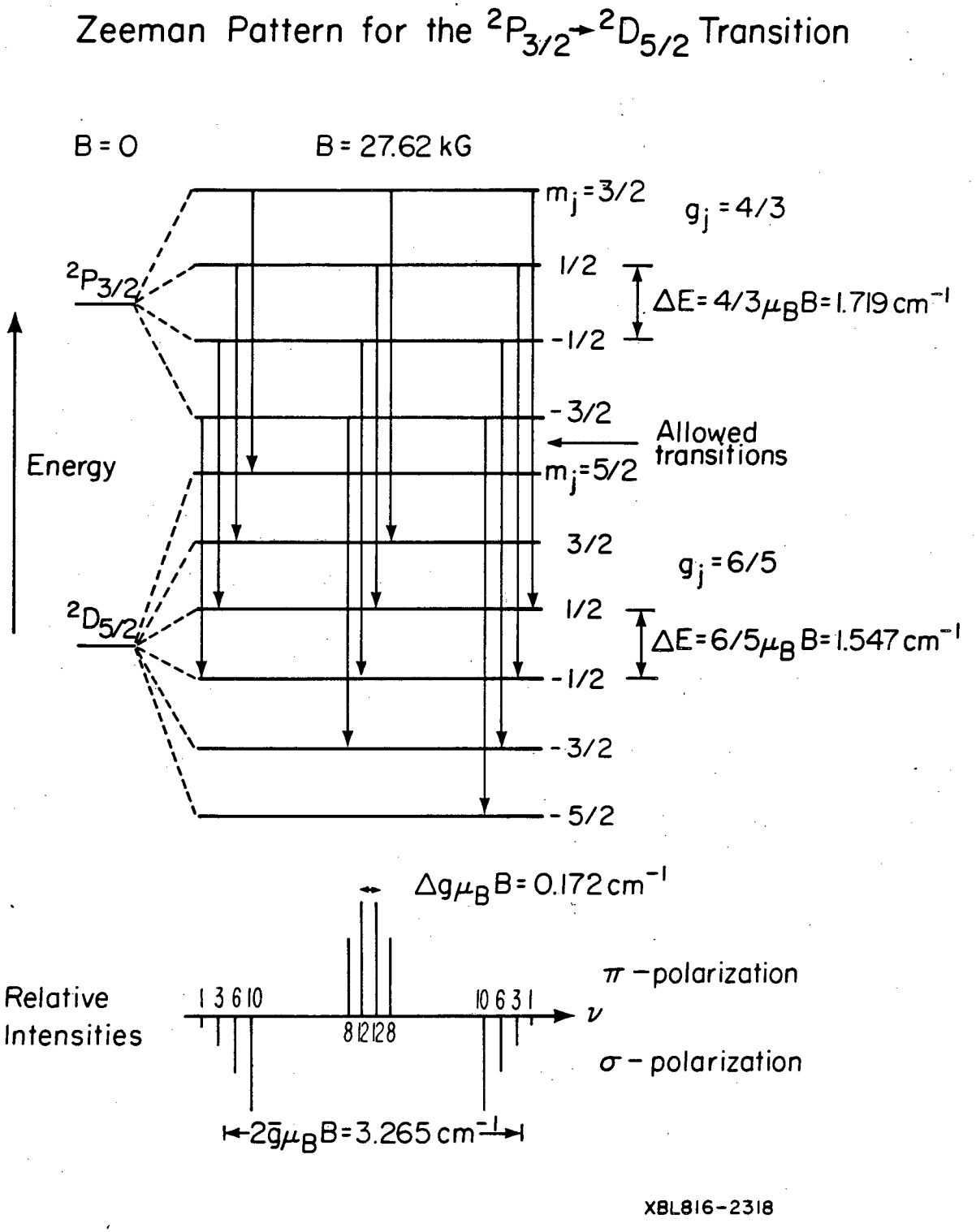

Figure IV.2. Zeeman pattern for the $^2P_{3/2}$ to $^2D_{5/2}$ transition.

IV.3. The 6p $^2P_{3/2}$ to 5d $^2D_{5/2}$ Transition

The sliding spark source was modified as previously described. Plates were taken for each fairly strong Nb V line in the 2500 to 4600 angstrom region. Only four of these strong lines were visible when the magnetic field was applied. The plates consisted of three pairs of tracks. One pair with the field off, and one pair for each polarization of the light with the field on. Each pair consisted of a niobium track and a thorium standard track. The light was polarized with a Nicol prism.

The CAS was used to make plots of intensity as a function of position in the vicinity of the lines of interest. Figure IV.3a is the π-polarized track and Figure IV.3b is the σ-polarized track for the 6p $^2P_{3/2}$ to 5d $^2P_{5/2}$ transition. It should be noted that the scatter in these plots is due to grain noise on the plate and not to problems with the data or their acquisition. Notice that in these plots the 'anomalous' structure is not at all visible. Therefore, the difference in g-values of the states cannot be found. The separation of the lines in the σ-polarized track (Figure IV.3b) is measured to be 2.579 cm^{-1} which is noticeably less than the 3.265 cm^{-1} indicated in Figure IV.2. This is a reasonable difference, however, because the more intense components of the anomalous structure are closer together. In fact, if one assumes that the pattern should be as it is shown in Figure IV.2, and that separation of the combined σ-polarized lines can be found by weighting the position of each component by its intensity, then this value of the splitting is only off by 9 percent.

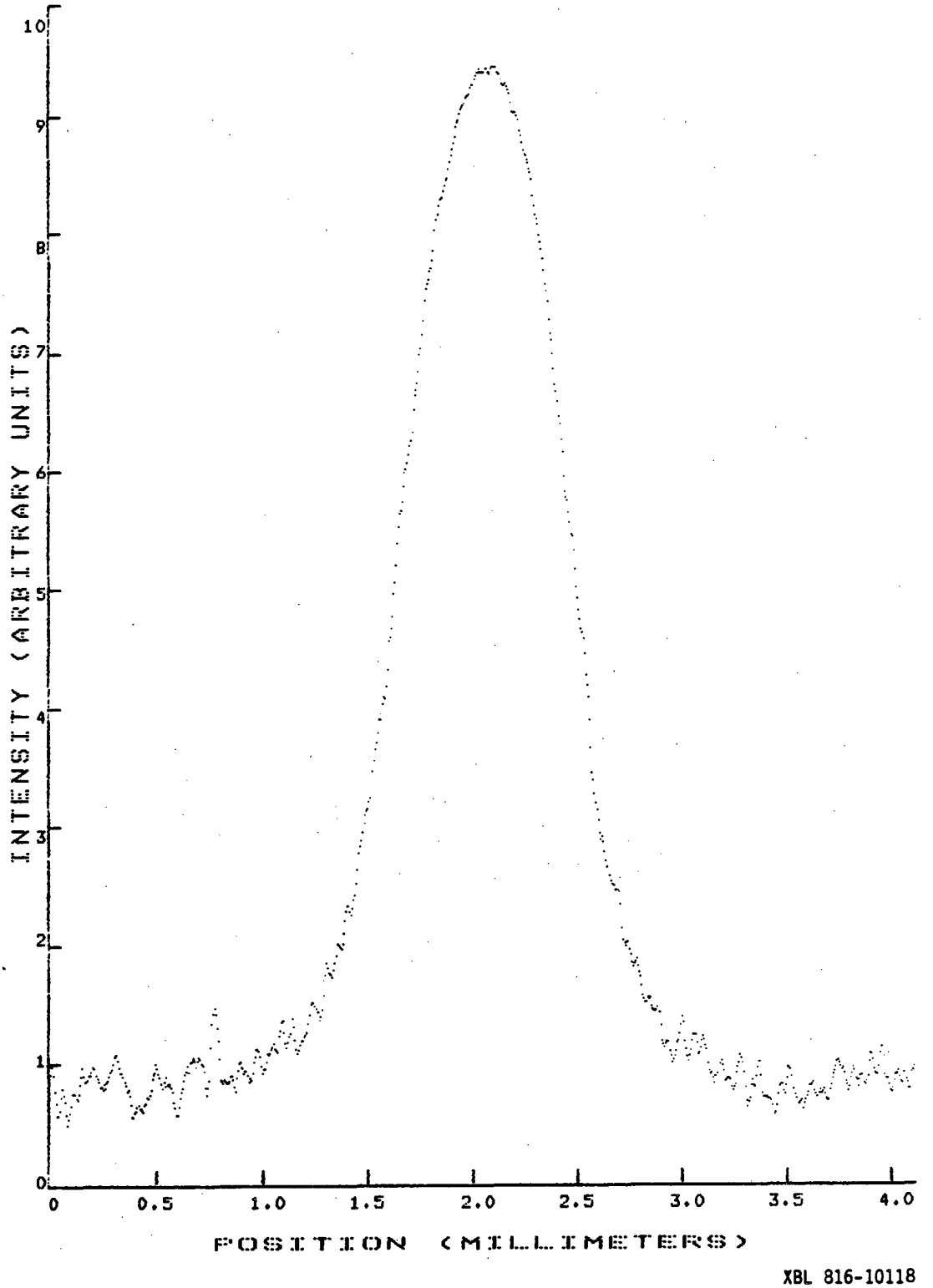

Figure IV.3a. C.A.S. densitometer tracing of the $^2P_{3/2}$ to $^2D_{5/2}$ transition.

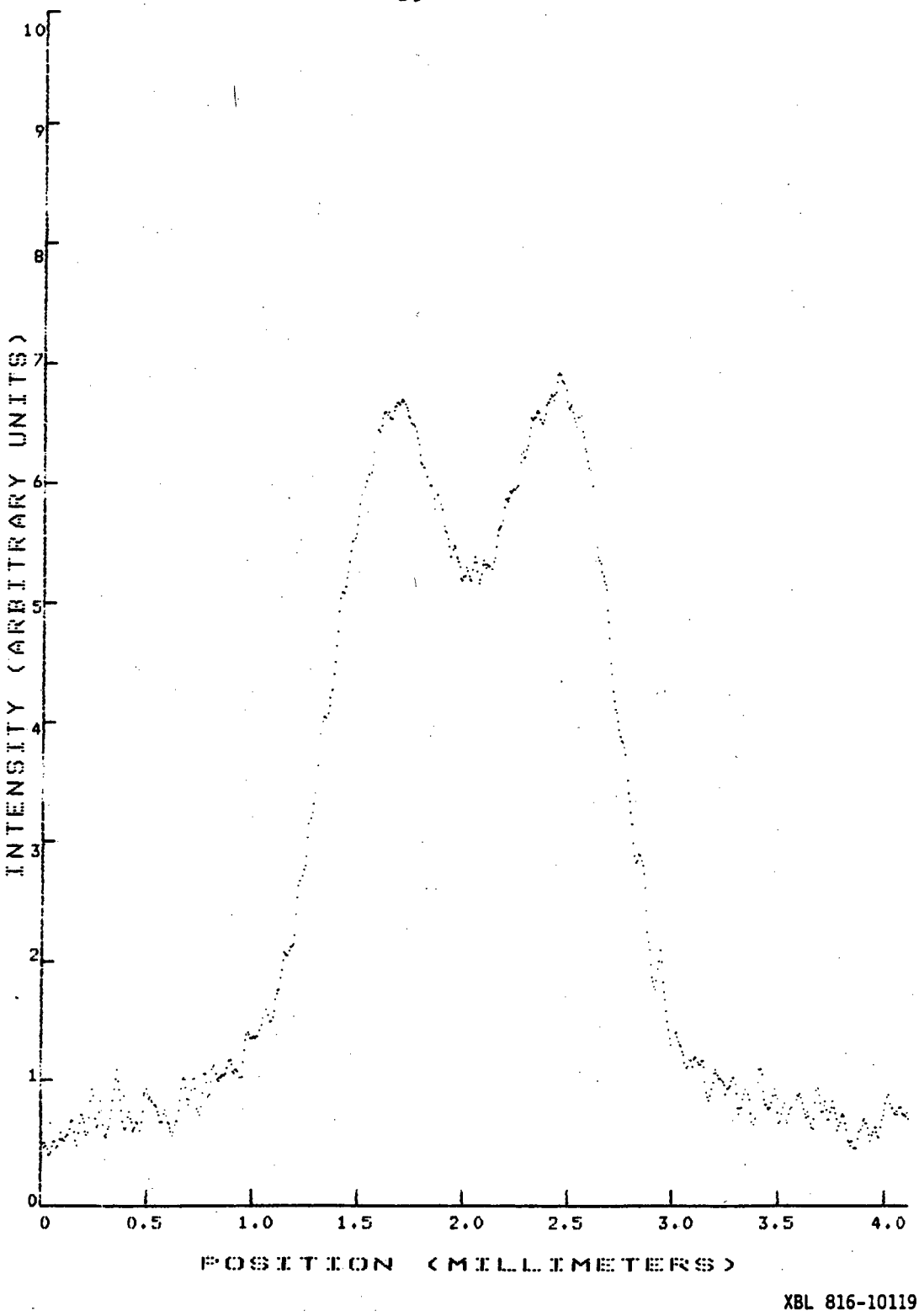

Figure IV.3b. C.A.S. densitometer tracing of the $^2P_{3/2}$ to $^2D_{5/2}$ transition.

IV.4. The 6h ^{2}H to 5g ^{2}G Transition

The fine structure splitting in the 5g ^{2}G and 6h ^{2}H levels is very small, especially when compared with the Zeeman splitting. This means that the assumption in Section IV.2.2 about the small mixing of the $|n,\ell,s,j,m_j\rangle$ wavefunctions does not hold and degenerate perturbation theory must be used. However, if one rewrites the Zeeman Hamiltonian of Section IV.2.1 as,

$$H = H_0 + \frac{eB}{2mc}(L_z + 2S_z)$$

and notices that if the fine structure term in H_0 is small, then one can use states of the form $|n,\ell,m_\ell,s,m_s\rangle$ as the eigenstates of H_0. Then the Zeeman energy shifts are,

$$\Delta E = \frac{eB}{2mc}\{\langle n,\ell,m_\ell,s,m_s|L_z|n,\ell,m_\ell,s,m_s\rangle + 2\langle n,\ell,m_\ell,s,m_s|S_z|n,\ell,m_\ell,s,m_s\rangle\}$$

The matrix elements are straight forward,

$$\Delta E = \frac{e\hbar B}{2mc}\{m_\ell + 2m_s\}$$

The allowed transitions are ones for which $\Delta m_s = 0$ and $\Delta m_\ell = 0$ or ± 1. The theoretical energy levels and allowed transitions are shown in Figure IV.4. Note that for this case, the splitting between the Zeeman levels in both the 5g ^{2}G and 6h ^{2}H levels is the same and is given by $\mu_B B$. Therefore, all of the 'anomalous' structure is gone. This means that in the π-polarized track there will be only one line at the same position as the transition in the zero field case and that in the σ-polarized track there will be just two lines each one separated from the zero-field line by $\mu_B B$.

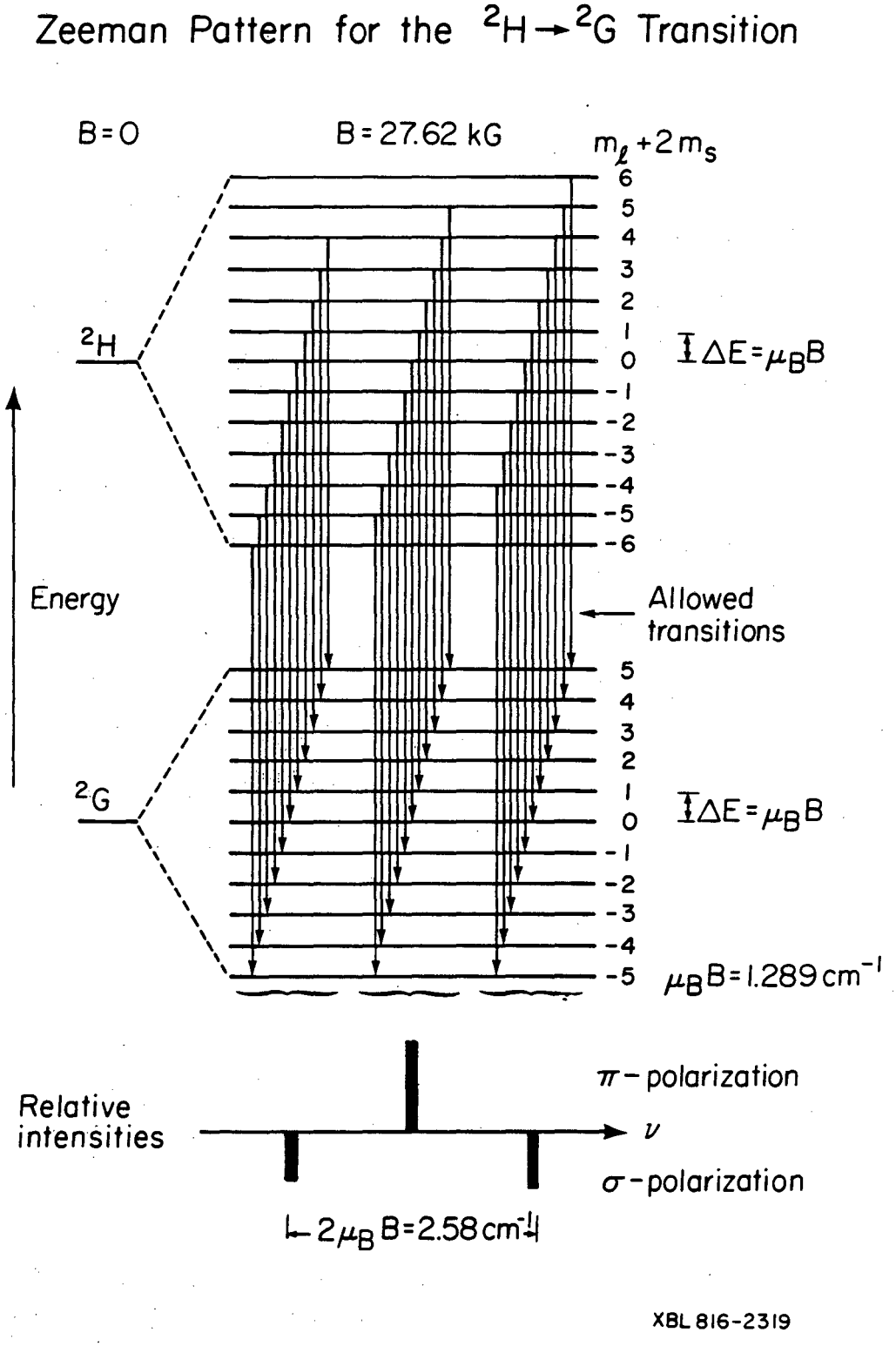

Figure IV.4. Zeeman pattern for the ^2H to ^2G transition.

The π-polarized tracing is shown in Figure IV.5a and the σ-polarized tracing is shown in Figure IV.5b. The measured splitting of the peaks in the σ-polarized track is 2.072 cm^{-1}. Correcting this value for the shift in the peaks due to their overlap, one finds that the separation of the individual lines is 2.746 cm^{-1}. This result is only 7 percent larger than the predicted value of 2.578 cm^{-1}.

IV.5. The Hyperfine Interaction in the 6p ^2P to 6s ^2S Transitions

The hyperfine splitting in the S-states of niobium atoms is generally quite large due to the large nuclear spin of niobium (I = 9/2). In Table III.2 the reader may have noticed that the hyperfine splitting in the 6s $^2S_{1/2}$ state is greater than 1 cm^{-1}. In the previous section, the typical Zeeman splitting was shown to be about 1.3 cm^{-1}. Therefore, the assumption about the small mixing of the wavefunctions is incorrect, and in fact, degenerate perturbation theory is needed to find the wavefunctions and energies in the magnetic field. The Hamiltonian for these S-states can be given by

$$H = H_0 + \lambda \vec{I}\cdot\vec{S} + \nu S_z$$

where $\vec{I}$ is the nuclear spin, $\vec{S}$ is the electron spin, and λ and ν are given by,

$$\lambda = \frac{16\pi}{3} \frac{e\hbar}{2mc} \frac{e\hbar}{2Mc} g_N \psi_0^2 \qquad \text{and} \qquad \nu = g_s \frac{e\hbar B}{2mc}$$

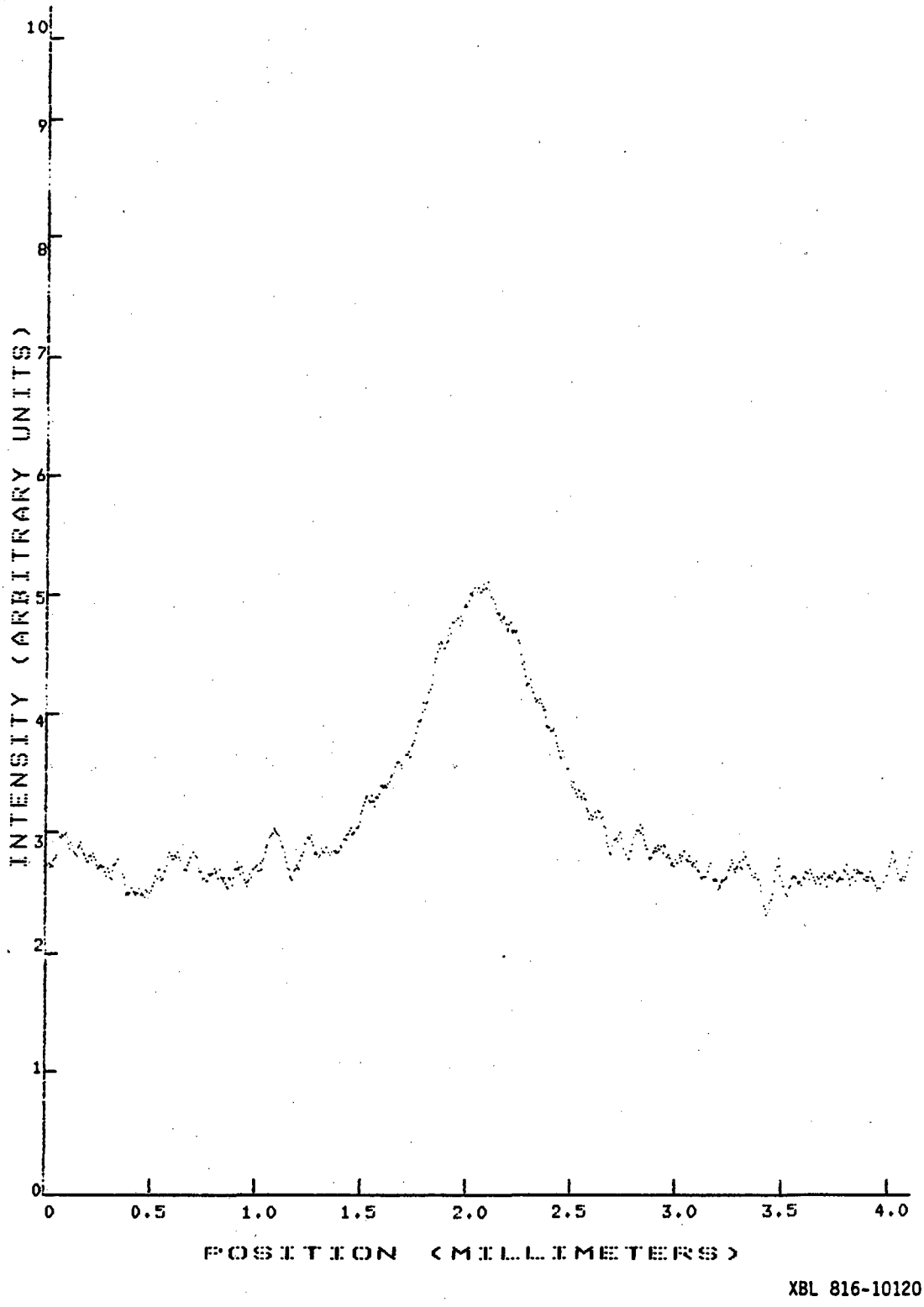

Figure IV.5a. C.A.S. densitometer tracing of the ^2H to ^2G transition.

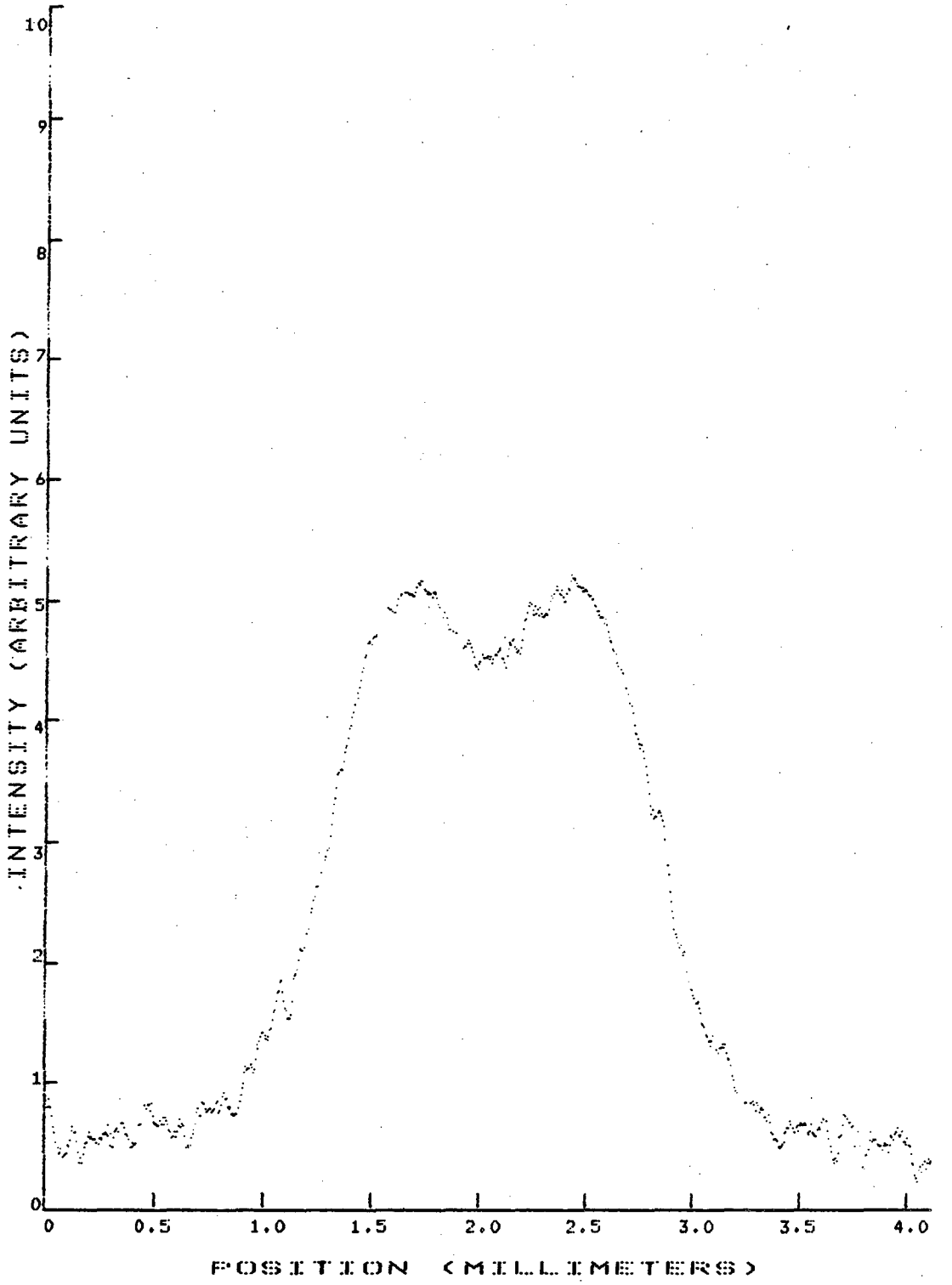

Figure IV.5b. C.A.S. densitometer tracing of the ^2H to ^2G transition.

where M is the nuclear mass, ψ_0^2 is the probability of finding the electron at the center of the nucleus, g_N is the nuclear g-factor (6.6167 for niobium), and g_s is 2. The second term in the Hamiltonian is from the nuclear spin interacting with the electron's spin (see Kuhn [1969]). The last term is due to the electron's spin interacting with the Zeeman field. It is the same as the term in the Zeeman Hamiltonian except that j=0 for the S-states being discussed here. The term that comes from the nuclear spin interacting with the Zeeman field has been neglected because it is 2000 times smaller than either of these terms.

Hamiltonians of the same form as the ones above are discussed by Merzbacher [1970]. The best wavefunctions for this Hamiltonian are ones in which the electron spin, s, and the nuclear spin, i, are coupled to give a total angular momentum, f. They are of the form,

$$|n,i,s,f,m_f\rangle$$

In the preceding section, degenerate perturbation theory was unnecessary because states of the same l, s, and m_j were assumed to be far apart in energy. Here, however, states of the same i, s, and m_f are quite close in energy. Therefore, to find the energy shifts of the states, for the s = 1/2 case, one must solve the determinmental equation,

$$\begin{vmatrix} \alpha - \Delta E & \gamma \\ \gamma & \beta - \Delta E \end{vmatrix} = 0$$

where

$$\alpha = \langle i,1/2,i+1/2,m_f | H' | i,1/2,i+1/2,m_f \rangle$$

$$\beta = \langle i,1/2,i-1/2,m_f | H' | i,1/2,i-1/2,m_f \rangle$$

$$\gamma = \langle i,1/2,i+1/2,m_f | H' | i,1/2,i-1/2,m_f \rangle$$

$$= \langle i,1/2,i-1/2,m_f | H' | i,1/2,i+1/2,m_f \rangle$$

$$H' = \lambda \vec{I} \cdot \vec{S} + \nu S_z$$

The energy shifts are then,

$$\Delta E_{m_f} = -\frac{\lambda}{4} \pm \frac{\nu}{2} \sqrt{1+2m_f\left(\frac{\lambda}{\nu}\right) + \left(\frac{2i+1}{2}\right)^2 \left(\frac{\lambda}{\nu}\right)^2}$$

For the case of s = 1/2, the matrix elements α, β, and γ are given by Merzbacher [1970],

$$\alpha = \frac{1}{2}\lambda + \frac{m_f}{2i+1}\nu$$

$$\beta = -\frac{i+1}{2}\lambda - \frac{m_f}{2i+1}\nu$$

$$\gamma = \frac{\sqrt{(i+1/2)^2 - m_f^2}}{2i+1}$$

For the case of i = 9/2,

$$\alpha = \frac{9}{4}\lambda + \frac{m_f}{10}\nu$$

$$\beta = -\frac{11}{4}\lambda - \frac{m_f}{10}\nu$$

$$\gamma = \frac{\sqrt{25 - m_f^2}}{10}$$

The energy shifts for the S-states are,

$$\Delta E_{m_f} = -\frac{\lambda}{4} \pm \frac{\nu}{2}\sqrt{1+2m_f(\frac{\lambda}{\nu})+25(\frac{\lambda}{\nu})^2}$$

and the wavefunctions are of the form,

$$|\psi\rangle = a|9/2,1/2,5,m_f\rangle + b|9/2,1/2,4,m_f\rangle$$

where

$$a^2 + b^2 = 1 \qquad \text{and} \qquad a^2 = \frac{\gamma^2}{\gamma^2+(\alpha-\Delta E_{m_f})^2}$$

To find the relative intensities of the transitions between the hyperfine levels, one must evaluate,

$$W = \langle n,\ell,s,j,i,f,m_f|\vec{r}|n',\ell',s',j',i',f',m_f'\rangle$$

Using the Wigner-Eckart theorem,

$$W = (-1)^{f-m_f} \begin{pmatrix} f' & 1 & f \\ -m_f' & q & m_f \end{pmatrix} \langle n,\ell,s,j,i,f\|r\|n',\ell',s',j',i',f'\rangle$$

where q=0 or ±1 depending on the polarization, and the six characters in the parentheses represent a 3-j symbol (Wigner coefficient). Since the matrix element on the right hand side of the expression above is not the same for all possible transitions (e.g., f=4, f'=4 transitions will give a different value than f=4, f'=5 or f=5, f'=5), it must be reduced further. Using the notation,

$$\langle\|r\|\rangle = \langle n,\ell,s,j,i,f\|r\|n',\ell',s',j',i',f'\rangle$$

One can show that (see Shore and Menzel [1968]),

$$\langle\|r\|\rangle = \delta_{ii'} \sqrt{f(f+1)f'(f'+1)}\ (-1)^{j+i+f'+1} \begin{Bmatrix} i & j & f \\ 1 & f' & j' \end{Bmatrix} \times \langle n,\ell,s,j\|r\|n',\ell',s'j'\rangle$$

where the six characters in the { } brackets are a 6-j symbol (Racah coefficient). Now the remaining matrix element is the same for all transitions in the Zeeman pattern and one may finally write,

$$W = (-1)^{f+f'+j+i+1-m_f} \delta_{ii'} \sqrt{f(f+1)f'(f'+1)} \begin{pmatrix} f' & 1 & f \\ -m_f' & q & m_f \end{pmatrix} \begin{Bmatrix} i & j & f \\ 1 & f' & j' \end{Bmatrix} \times \langle n,\ell,s,j\|r\|n',\ell',s',j'\rangle$$

There exist computer programs for calculating the 3-j and 6-j symbols that are needed. However, as the reader may have already noted, these calculations will only give information on the detailed structure of the pattern (similar to the 'anomalous' Zeeman structure). Since the Doppler broadening of the lines makes study of this structure nearly impossible, the benefits of completing this calculation are dubious.

Figure IV.6 is an energy level diagram for the $^2P_{1/2}$ to $^2S_{1/2}$ transition. Notice that applying the Zeeman field to the previously split hyperfine levels of the $^2S_{1/2}$ state causes an apparent increase in the separation of the levels and a smaller smearing of them. Zero field levels from both hyperfine states contribute to each collection of levels in the Zeeman field. The calculations for the energies in Figure IV.6 were based on a hyperfine splitting of 1.1 wavenumbers and a magnetic field of 27.62 kilogauss. While the details of the line profiles were not calculated, one might suspect that the separation of the lines in the σ-polarized track would be increased relative to the splitting that one would expect if there were no hyperfine interaction. Indeed, this turns out to be the case. The splitting of the lines in the σ-polarized track (Figure IV.7b) is 3.550 cm^{-1} as opposed to the 3.437 cm^{-1} that one would expect if the hyperfine interaction were negligible. This is also true for the splitting of the lines in the π-polarized track (Figure IV.7a). The measure separation is 1.832 cm^{-1} and the expected value with no hyperfine interaction is 1.719 cm^{-1}.

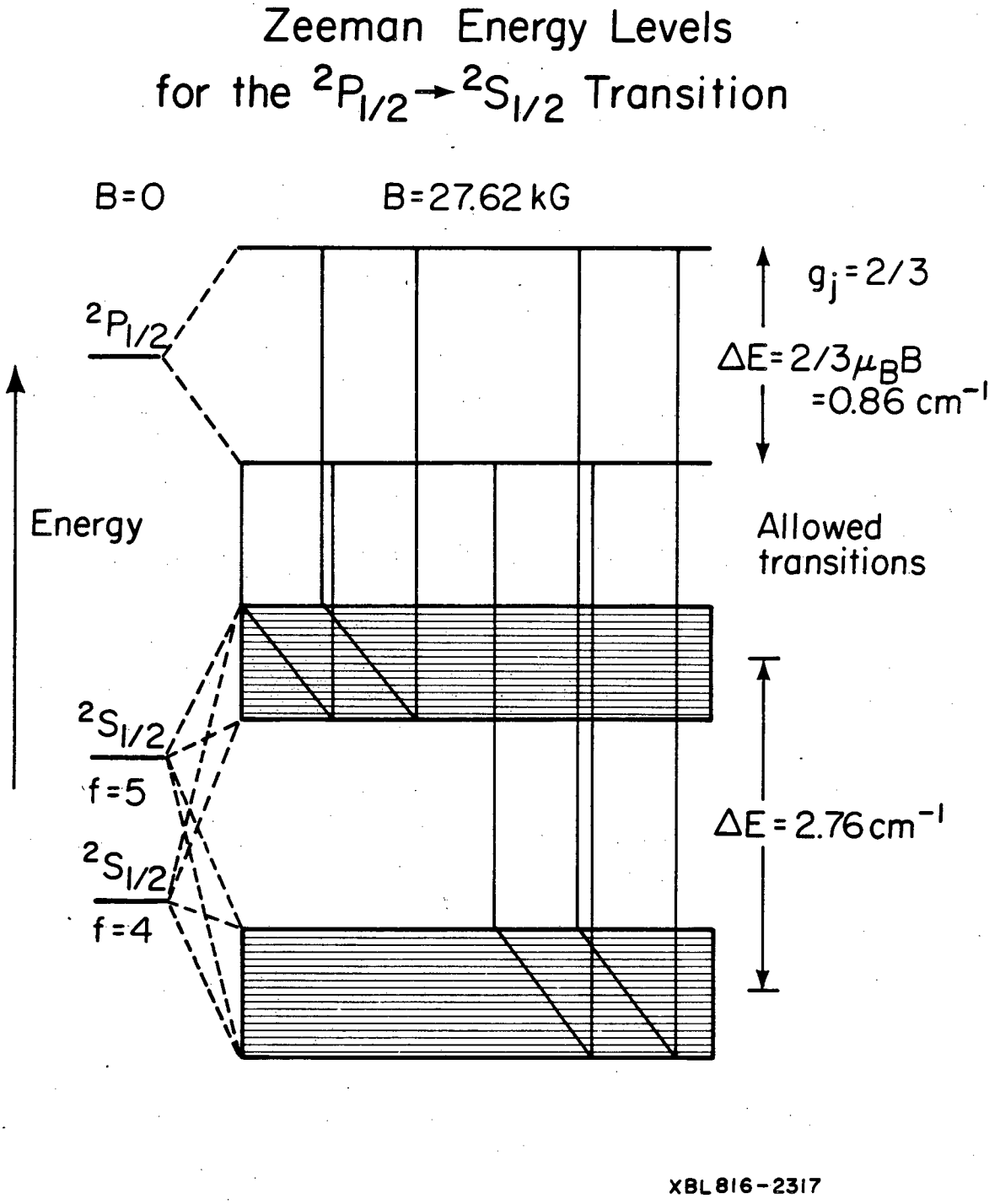

Figure IV.6. Zeeman energy levels for the $^2P_{1/2}$ to $^2S_{1/2}$ transition.

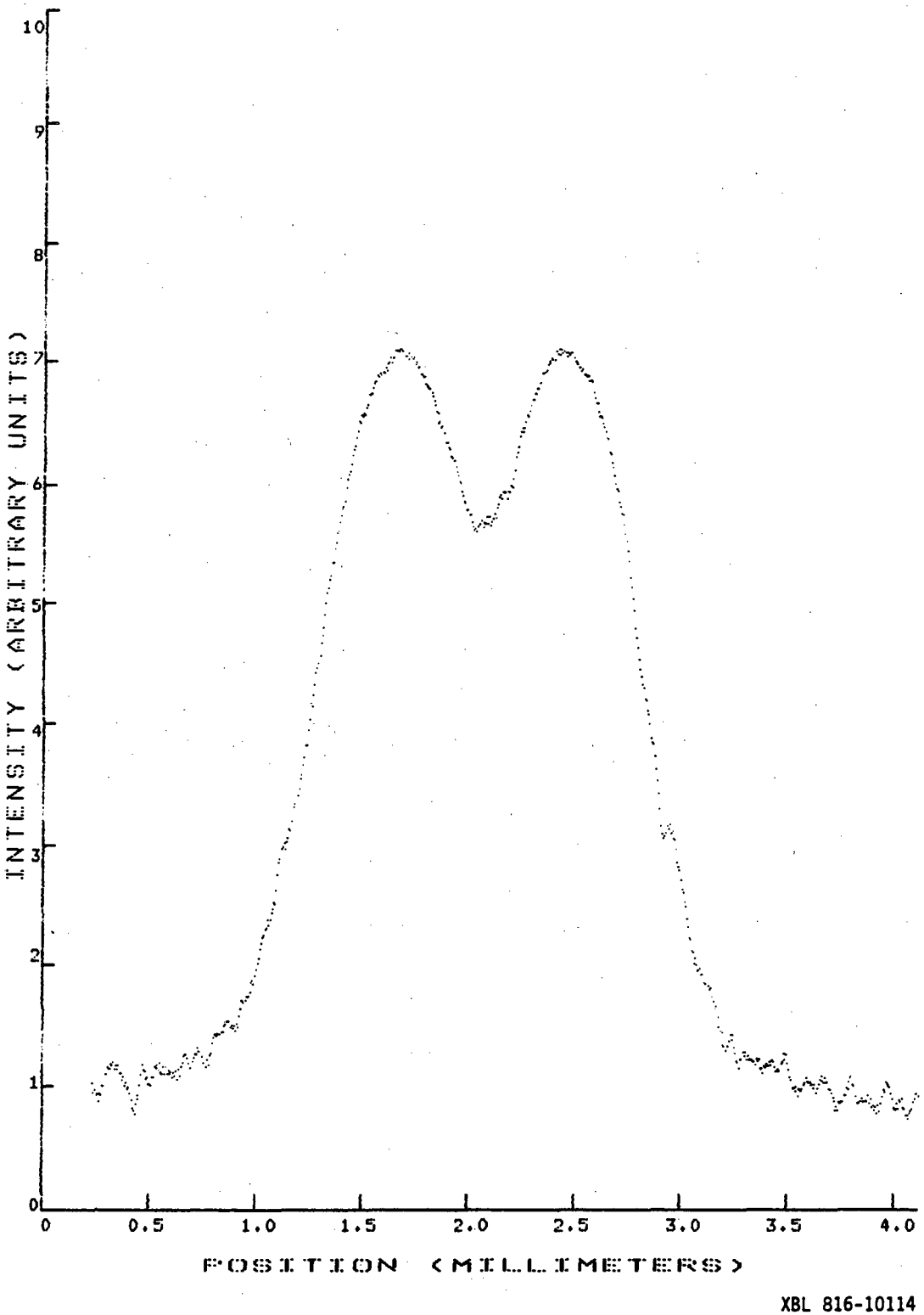

Figure IV.7a. CA.S. densitometer tracing of the $^2P_{1/2}$ to $^2S_{1/2}$ transition.

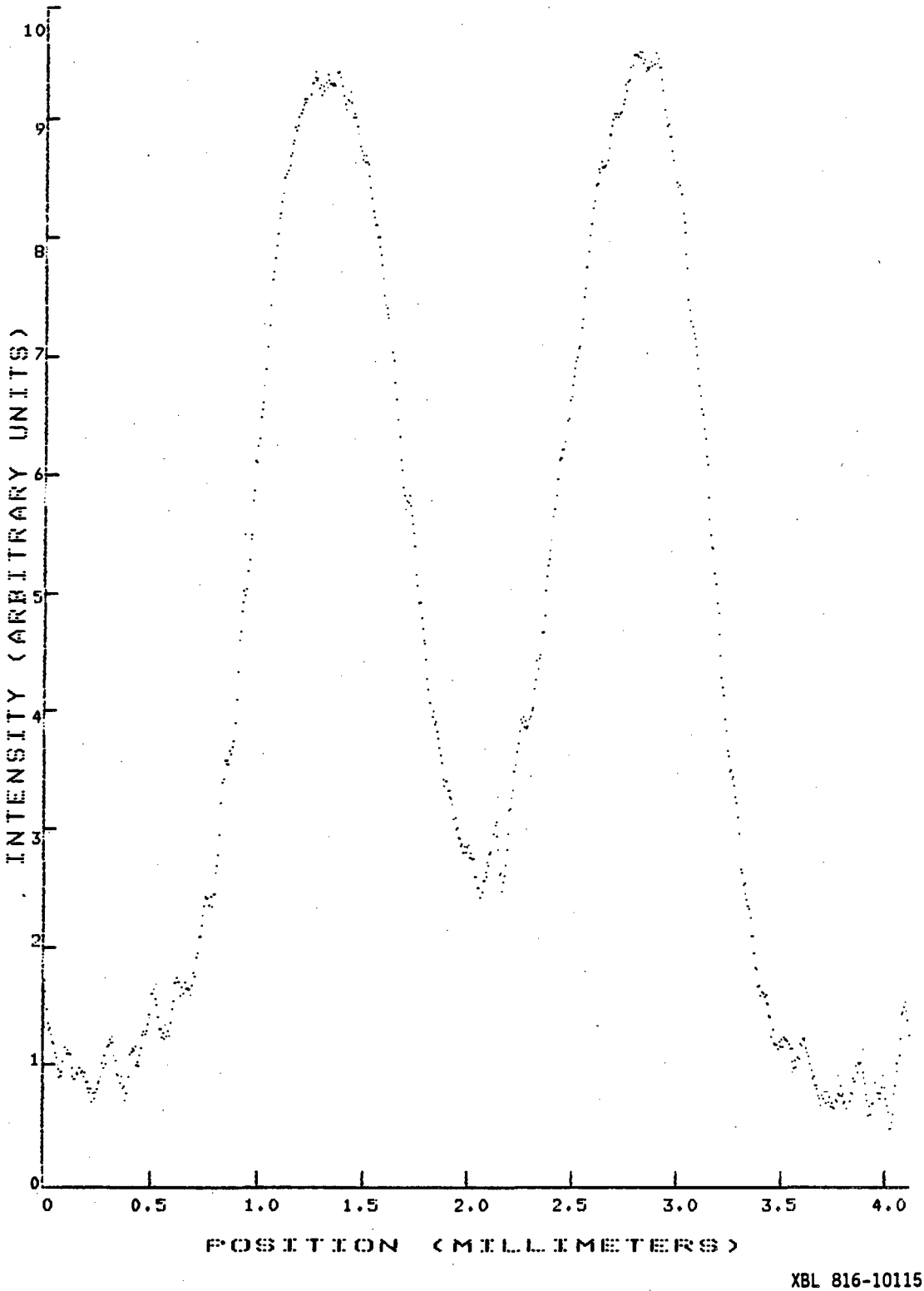

Figure IV.7b. C.A.S. densitometer tracing of the $^2P_{1/2}$ to $^2S_{1/2}$ transition.

The tracings for the $^2P_{3/2}$ to $^2S_{1/2}$ transitions are shown in Figures IV.8a and IV.8b. Notice that they are much broader than the corresponding tracing for the $^2P_{1/2}$ to $^2S_{1/2}$ transitions. This is because the $^2P_{3/2}$ level now is split into 4 levels by the magnetic field and each level has transitions to the $^2S_{1/2}$ levels.

IV.6. A Discussion of Problems and Suggestions for Future Work

While the results of this study are generally in agreement with standard atomic theory, they are somewhat disappointing. Most of the problems stem from the rather large width of the lines, which masks almost completely the 'anomalous' structure. The only solution for this problem is to change the source in some convenient, but useful manner. Good suggestions for source improvements are hard to come by, because any spark source that can produce four-times ionized species is going to have a rather large Doppler width for its spectra. The best possibility for continuing this work most certainly will require a different type of source, possibly an ion trap of some sort.

Putting the problem of a suitable source aside this project holds some interesting results. In this single electron spectrum, one can see a large range of different atomic interactions. These include the interaction of a hyperfine energy on the order of the Zeeman splitting and the Zeeman effect over the range of very small to very large fine-structure intervals.

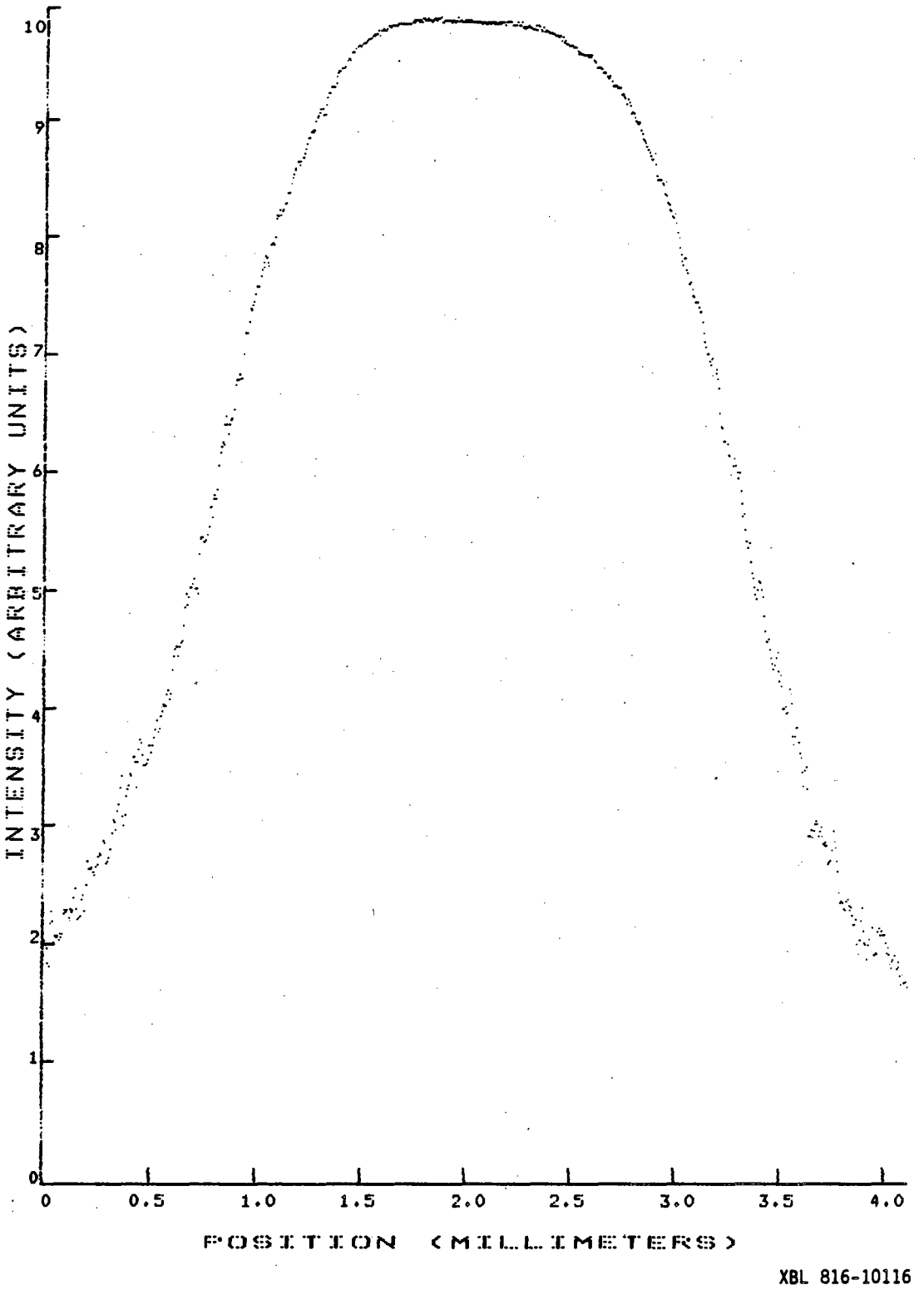

Figure IV.8a. C.A.S. densitometer tracing of the $^2P_{3/2}$ to $^2S_{1/2}$ transition.

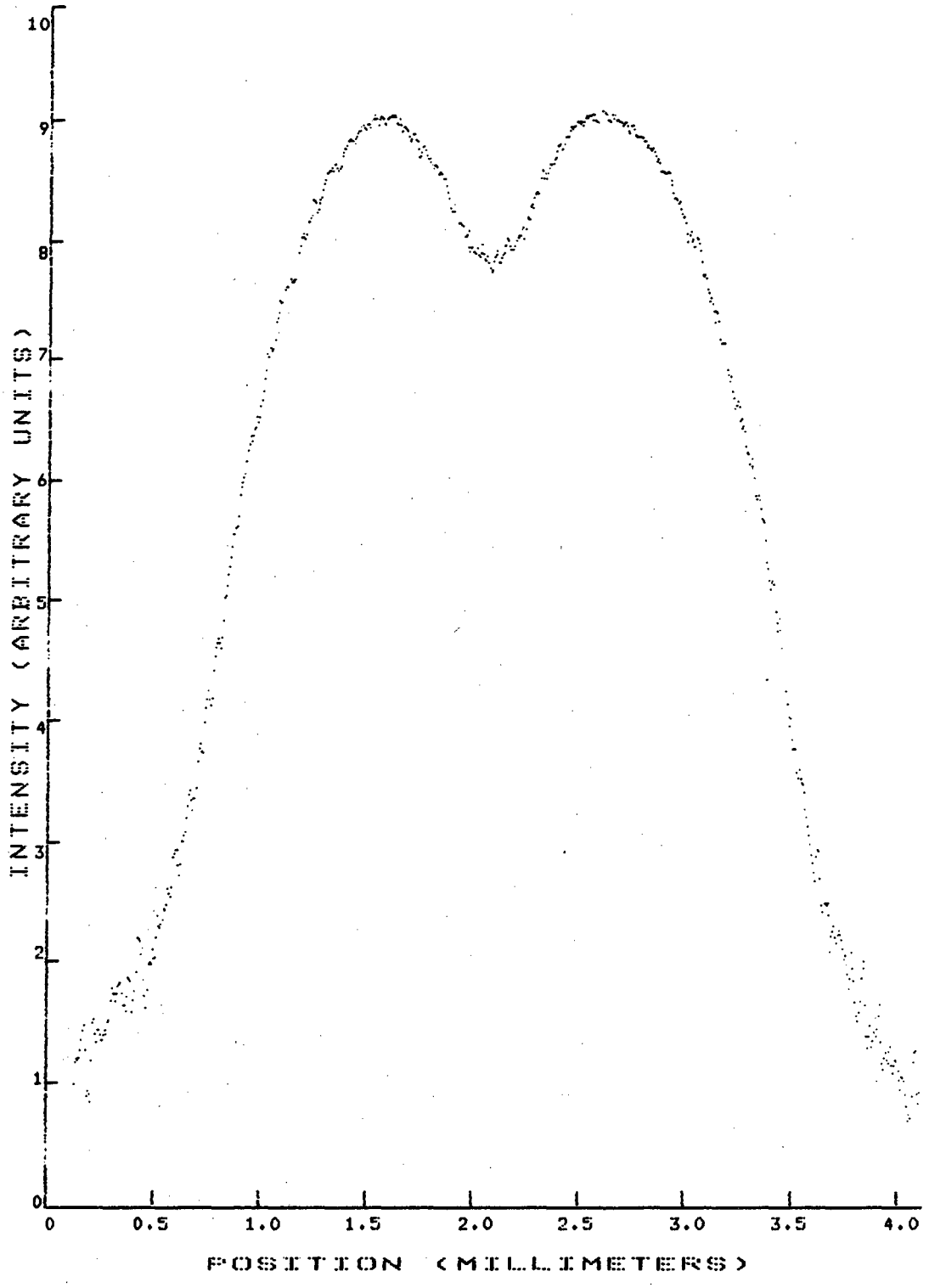

Figure IV.8b. C.A.S. densitometer tracing of the $^2P_{3/2}$ to $^2S_{1/2}$ transition.

V. LASER MODIFICATION OF THE POPULATIONS OF CERTAIN LEVELS IN THE SLIDING SPARK SOURCE

V.1. Introduction

It was the experience of the author, as well as that of Van Deurzen [1977], that the intensity of transitions between states of high angular momentum ($\ell>3$) where $\ell=n-1$, was extremely large. Part of this effect is due to the similarity of the wavefunctions of the states $|n,\ell,s,j,m_j\rangle$ and $|n+1,\ell+1,s,j+1,m_j'\rangle$, but it also seems that the sliding spark source has some mechanism for preferentially populating the states with $\ell=n-1$ and large ℓ.

If this population effect is real, one could gain intensity in other transitions by using a laser to drive the atoms on the $\ell=n-1$ edge over to other states that seem to be under-populated. The result of this population shift is two-fold; first, it could increase the intensity of transitions that were difficult to find, and second, provide some data on the connection of certain atomic levels.

V.2. Theory

The transition rate between two states is proportional to the matrix element,

$$W = \langle n,\ell,s,j,m_j|\vec{r}|n',\ell',s',j',m_j'\rangle$$

This matrix element will, of course, be largest when the two states involved have similar wavefunctions. For one electron atoms, one may recall that the number of nodes in the radial part of the wavefunction

is $n-\ell-1$. The matrix element then, will generally be largest for states with no nodes because then the integrand is positive definite. This means that transitions between states with $\ell=n-1$ will have rather large transition probabilities. However, the total intensity of a transition also depends on the populations of the levels involved.

The relationship between the population of the atomic levels 1 and 2 and the density of radiation at the frequency of transition is given by (see Thorne [1974]),

$$N_2(A + \rho B_{21}) = N_1 \rho B_{12}$$

where N_1 is the population of level 1, N_2 is the population of level 2, A is the spontaneous transition probability from level 2 to level 1, B_{21} is the probability of stimulated emission from level 2 to level 1, B_{12} is the absorption probability from level 1 to level 2, and ρ is the density of radiation at the frequency of transition between levels 1 and 2. While this relation is usually derived classically, Sakurai [1967] derives it rigorously using quantum field theory.

If one applies a laser at the wavelength that connects the two levels, the density becomes extremely large and therefore A becomes negligible compared to ρB_{21}. Since B_{12} is about the same size as B_{21}, the populations of the levels tend to equalize. In the case considered here, one can use this method to drive the ions from the $\ell=n-1$ edge to other less populated states.

V.3. The Experiment

The best set of transitions for conducting this experiment in Nb V are shown in Figure V.1. The 5g ^2G levels are on the $\ell=n-1$ edge. They are connected to the 6f $^2F_{7/2}$ level by a transition at 3998.6 Å. This transition was driven with a dye laser, and fluorescence at 2883.5 Å from the 6f $^2F_{7/2}$ level to the 6d D level was searched for.

Light at 3998.6 Å is about in the center of the lasing range of the dye PBBO (2-(4'-Biphenylyl)-6-phenylbenzoxazole). This dye was used in a Molectron DL-100 tunable dye laser which was pumped by a Molectron UV14 Nitrogen Laser. The pulse energy of this dye was around 300 microjoules emitted over about 10 nanoseconds. The laser was triggered by the same circuitry that fired the sliding spark source, but the laser pulse could be delayed with respect to the current pulse for the source. The laser light was sent through the source at various intervals after the current pulse was fired. The interval ranged from 10 to 50 microseconds.

The light from the source was sent into the 3.4 meter Ebert spectrograph, and photographed on a spectroscopic plate. The plate contained 5 pairs of tracks, each for a different time delay. Each pair consisted of a track with the laser on and a track with the laser off.

V.4. The Results and Problems

The track to track variations in the darkening of the emulsion were greater than any real fluorescence effect. This was most likely due to fluctuations in the source rather than fluctuations in the plate. The

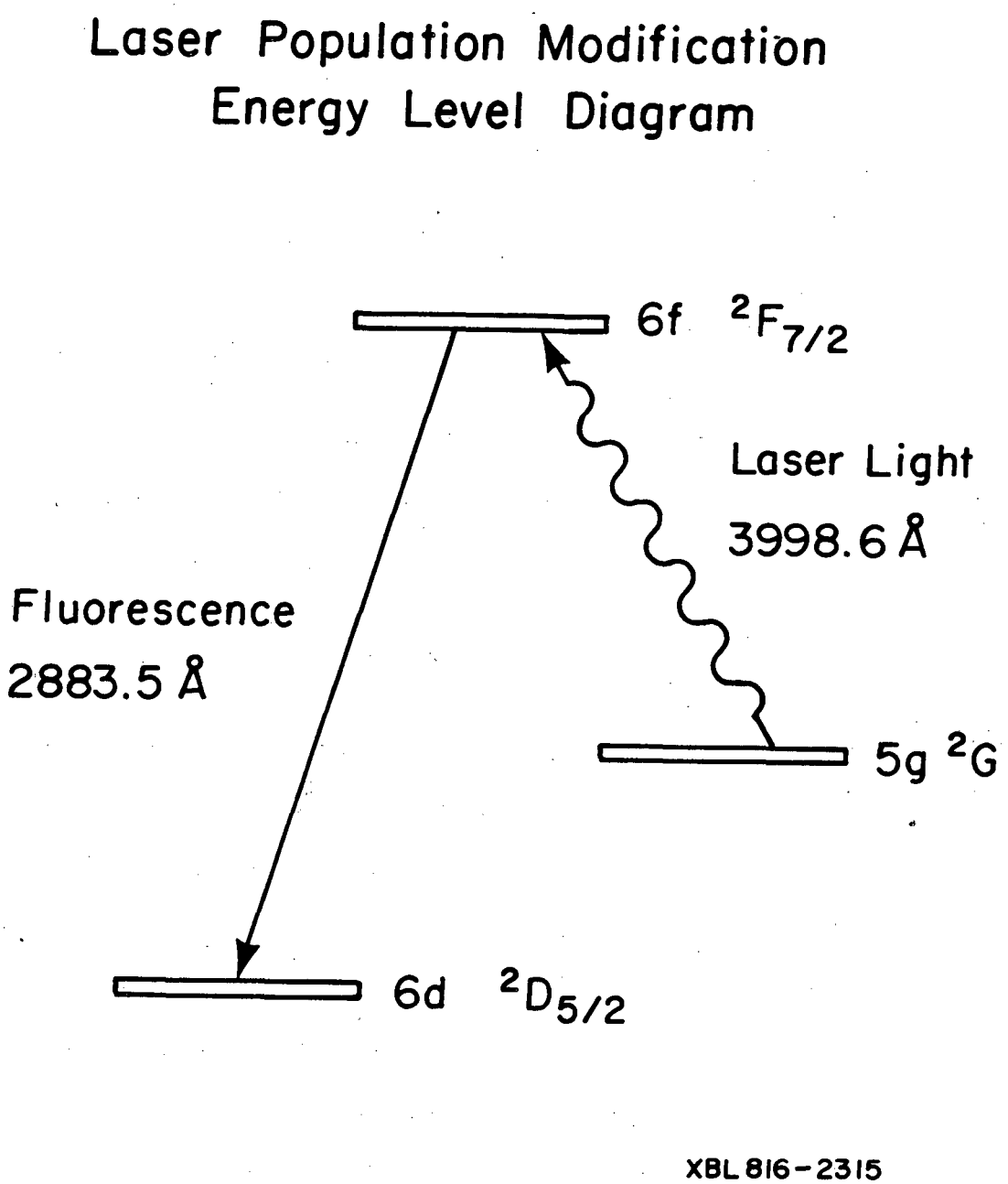

Figure V.1. Laser population modification energy level diagram.

results (or lack thereof) indicate one of three things. First, the indicated level assignments could be wrong. This is unlikely because these levels fit quite well into the energy level scheme for the fifth spectrum of niobium. The second possibility is that the 5g ^2G level really isn't over-populated. The last explanation is that the laser wasn't intense enough to drive a substantial fraction of the 5g ^2G level's population over the 6f $^2F_{7/2}$ level. This is the most reasonable idea. The ratio of the constants A and B_{21} is always,

$$\frac{A}{B_{21}} = \frac{8\pi h}{\lambda^3}$$

For the transition in question this ratio is about 10^{-13}. If one assumes that the laser's peak energy per unit volume is about 10^{-1} joules per cubic meter (this is about 300 microjoules in a 10 nanosecond pulse in a 3 mm diameter beam), and that the 5g ^2G-6f $^2F_{7/2}$ transition has a width of about 0.5 Å, then ρ is only about 10^{-12} over the 10 nano-second period. This means that indeed the laser is not going to change the populations significantly over the 100 microsecond lifetime of the spark. Therefore, to properly conduct this experiment one needs either a continuous laser or a mechanism for examining only the 10 nanoseconds of the spark that the laser effects.

VI. CONCLUSIONS

The nearly unperturbed levels of the $4p^6n\ell$ configuration of four-times ionized niobium have now been found and classified. The line list of Trawick [1934] and Charles [1950] has now been expanded from the original 13 lines to 84 lines in the wavelength region between 300 Å and 5400 Å. This line list was used to find the energy levels of this configuration and yields values for 30 of them. The ionization energy of four-times ionized niobium was also estimated from these data and was found to be 407897 cm^{-1}. In addition, the hyperfine splitting of the 5s $^2S_{1/2}$ and 6s $^2S_{1/2}$ levels was observed. The 6s $^2S_{1/2}$ splitting was measured to be 1.1 cm^{-1}. There was strong evidence for configuration mixing between the $4p^6nf$ levels and another even parity level. The most likely candidate for the mixing level is the $4p^54d^2$ level.

Future work on this spectrum should include studies of the other low-lying configurations, namely $4p^54d^2$, $4p^55s^2$, and $4p^54d5s$. This is a long and involved project because these levels aren't well known in the rubidium iso-electronic sequence. To continue it may be necessary to study these configurations throughout the entire iso-electronic sequence.

The Zeeman studies were not as successful as one might have hoped, however, there was no evidence for a wrong assignment of any of the lines that were investigated. There is a lot of interesting atomic physics going on when four-times ionized niobium is in a magnetic field, but the large width of the lines hides much of it.

The attempt to modify the population of various atomic levels in the sliding spark source is another experiment that is quite interesting, but the experimental technique must be refined. Two suggestions were put forward. First, a continuous laser could be used, or secondly, a sector wheel or similar device might be employed to examine the spark only when it is being irradiated by the pulsed laser.

ACKNOWLEDGMENTS

I wish to thank, first of all, my thesis advisor, Sumner Davis for this help, guidance, and patience throughout my time at the University of California. In addition, I want to thank John Conway and George Shalimoff for the use of their facilities, large amounts of good advice, and a great willingness to help. Erna Meinders is to be thanked for providing the wavelengths mentioned in the text. I want to express many thanks to Normal Edelstein for supplying funds.

Cornelius Van Deurzen, Tom Hayhurst, Bruce Lulu, and Phil Hammer all deserve thanks for their good council and sage advice on many matters, usually, but not always related to this work. Also, I want to convey many thanks to the technical groups at Lawrence Berkeley Laboratory, especially to the following gentlemen and their staffs, Ed Voronin (machine shop), Larry Ornelas (machine shop), Fred Vogelsberg (electronics), Joe Katz (electronics), and Dane Anderberg (glass shop). Also, thanks to Bob Sedlak of the Physics Department glass shop for all of his efforts.

Finally, I wish to thank my wife, Carol Kirk, for having the patience and understanding to put up with me throughout these last few traumatic years.

This work was supported by the Director, Office of Energy Research, Office of Basic Energy Sciences, Chemical Sciences Division of the U.S. Department of Energy under Contract W-7405-ENG-48.

REFERENCES

G. Balloffet and J. Romand, J. Phys. 16, 490 (1955).

G. Balloffet and J. Romand, C. R. Acad. Sci. 242, 2333 (1956).

V. Barger and M. Olsson, "Classical Mechanics: A Modern Perspective," McGraw-Hill, New York, 1973, pp. 17-23.

R. E. Beverly III, "Light Emission from High-Current Surface-Spark Discharges," in Progress in Optics XVI, E. Wolf ed., North Holland, New York, 1978.

K. Bockasten, Ark. Fys. 9, 457 (1955).

M. S. Chaghtai, J. Opt. Soc. Am., 59, 969 (1969).

G. W. Charles, Phys. Rev. 77, 120 (1950).

E. U. Condon and G. H. Shortley, "The Theory of Atomic Spectra," Cambridge University Press, New York, 1970.

B. Edlen, Handb. d. Phys., 27, 80-220 (Berlin: Springr-Vergag 1964).

G. L. Epstein and J. Reader, J. Opt. Soc. Am., 65, 310 (1975).

M. Evan-Zohar and B. S. Fraenkel, J. Phys. B, 5, 1596 (1972).

A. Giacchetti, R. W. Stanley, and R. Zalubas, J. Opt. Soc. Am., 60, 474 (1970).

D. Griffin, "Self-Consistent Field Calculations of Excited Electronic Configurations," University Microfilms, Ann Arbor, Michigan, 1970.

G. R. Harrison, "M.I.T. Wavelength Tables," John Wiley and Sons, New York, 1939.

C. J. Humphreys and W. F. Meggers, J. Res. N. B. S. 34, 477 (1945).

L. Iglesias, J. Opt. Soc. Am., 45, 856 (1955).

V. Kaufman and B. Edlen, J. Phys. Chem. Ref. Data, 3, 825 (1974).

R. L. Kelly and L. J. Palumbo, "Atomic and Ionic Emission Lines Below 2000 Å," U.S. Government Printing Office, Washington, D. C., 1973.

C. C. Kiess, J. Res. N. B. S., 56, 167 (1956).

"Kodak Plates and Films for Scientific Photography," Eastman Kodak Company, Rochester, New York, 1973.

H. B. Kuhn, "Atomic Spectra," Academic Press, New York, 1969.

R. J. Lang, Zeeman Verhandelingen, p. 44, Martinus Nijhoff, The Hague, 1935.

B. A. Lulu, "The Zeeman Spectrum of Scandium," LBL Report 11407, 1980.

E. Merzbacher, "Quantum Mechanics," J. Wiley & Sons, New York, 1970.

C. E. Moore, "Atomic Energy Levels," Natl. Bur. Std. (U.S.), Circ. No. 467, U.S. Government Printing Office, Washington, D. C., 1949.

A. Mushtaq, M. S. Z. Chaghtai, and K. Rahimullah, J. Phys. B, 12, 19 (1979).

T. Preston, Phil. Mag., 45, 325 (1898).

L. J. Radziemski, K. J. Fisher, and D. W. Steinhaus, "Calculation of Atomic-Energy-Level Values," Los Alamos Laboratory Report (LA-4402, UC-34 Physics, TID-4500), 1970.

J. Reader, G. L. Epstein, and J. O. Ekberg, J. Opt. Soc. Am. 62, 273 (1972).

J. Romand and G. Balloffet, J. Phys. 16, 489 (1955).

N. P. Romanov and A. R. Striganov, Optics and Spect., 27, 8 (1969).

J. J. Sakurai, "Advanced Quantum Mechanics," Addison-Wesley, Menlo Park, California, 1967.

R. A. Sawyer, "Experimental Spectroscopy," Prentice-Hall, New York, 1964.

B. W. Shore and D. H. Menzel, "Principles of Atomic Spectra," John Wiley and Sons, New York, 1968.

A. P. Thorne, "Spectrophysics," Chapman and Hall, London, 1974.

M. W. Trawick, Phys. Rev., 46, 63 (1934).

G. E. Uhlenbeck and S. Goudsmit, Naturwissenschaften, 13, 953 (1925).

C. H. H. Van Deurzen, "Excitation Energies in an Electrically Pulsed Light-Emission Source Applied to the Separation of Higher Ionized Atomic States: Spectra and Energy Levels of Scandium 2+ and Vanadium 4+", LBL Report 1657, 1973.

C. H. H. Van Deurzen and J. Conway, Appl. Spectr., 28, 223 (1974).

C. H. H. Van Deurzen, J. Opt. Soc. Am. 67, 476 (1977).

B. Vodar and N. Astoin, Nature 166, 1029 (1950).

H. E. White, "Introduction to Atomic Spectra," McGraw-Hill, New York, 1934.

P. Zeeman, Phil. Mag., 5, 43, 226 (1897).

This report was done with support from the Department of Energy. Any conclusions or opinions expressed in this report represent solely those of the author(s) and not necessarily those of The Regents of the University of California, the Lawrence Berkeley Laboratory or the Department of Energy.

Reference to a company or product name does not imply approval or recommendation of the product by the University of California or the U.S. Department of Energy to the exclusion of others that may be suitable.

TECHNICAL INFORMATION DEPARTMENT
LAWRENCE BERKELEY LABORATORY
UNIVERSITY OF CALIFORNIA
BERKELEY, CALIFORNIA 94720